# Tropical and Extratropical Controls of Gulf of California Surges and Summertime Precipitation over the Southwestern United States

SALVATORE PASCALE AND SIMONA BORDONI

*California Institute of Technology, Pasadena, California*

(Manuscript received 6 December 2015, in final form 17 March 2016)

ABSTRACT

In this study ERA-Interim data are used to study the influence of Gulf of California (GoC) moisture surges on the North American monsoon (NAM) precipitation over Arizona and western New Mexico (AZWNM), as well as the connection with larger-scale tropical and extratropical variability. To identify GoC surges, an improved index based on principal component analyses of the near-surface GoC winds is introduced. It is found that GoC surges explain up to 70% of the summertime rainfall over AZWNM. The number of surges that lead to enhanced rainfall in this region varies from 4 to 18 per year and is positively correlated with annual summertime precipitation. Regression analyses are performed to explore the relationship between GoC surges, AZWNM precipitation, and tropical and extratropical atmospheric variability at the synoptic (2–8 days), quasi-biweekly (10–20 days), and subseasonal (25–90 days) time scales. It is found that tropical and extratropical waves, responsible for intrusions of moist tropical air into midlatitudes, interact on all three time scales, with direct impacts on the development of GoC surges and positive precipitation anomalies over AZWNM. Strong precipitation events in this region are, however, found to be associated with time scales longer than synoptic, with the quasi-biweekly and subseasonal modes playing a dominant role in the occurrence of these more extreme events.

## 1. Introduction

The seasonal cycle of rainfall over northwestern Mexico and the southwestern United States is dominated by the North American monsoon (NAM), a distinctive summertime circulation characterized by the following features: a sharp rainfall increase in early July after a very dry June (Higgins et al. 1997), the establishment of a mid- to upper-level monsoon anticyclone centered over New Mexico (Adams and Comrie 1997), a reversal in lower-level winds from northwesterly to southeasterly (Douglas 1995; Bordoni et al. 2004), and a marked warming of Gulf of California (GoC) waters, with sea surface temperatures (SSTs) reaching or even exceeding everywhere 30°C (Erfani and Mitchell 2014). The NAM precipitation accounts for as much as approximately 70% of the total annual rainfall in northwestern Mexico, the core monsoon region, and for approximately 40%–50% in the southwestern United States, its northernmost extremity (Douglas et al. 1993; Anderson et al. 2000) Hence, this system plays an important role in sustaining water resources and ecosystems in these regions.

Far from being a steady circulation, the NAM features subseasonal variability on different time scales. One important mode of variability that has received attention in the literature since the early 1970s (Hales 1972; Brenner 1974) is associated with transient disturbances traveling along the GoC. These disturbances, named GoC surges, appear as pronounced periods of anomalous northward winds and moisture transport along the GoC (e.g., Adams and Comrie 1997; Stensrud et al. 1997; Douglas et al. 1993; Bordoni et al. 2004) and are often followed by enhanced convective activity over Arizona and western New Mexico (hereafter AZWNM) (Higgins et al. 2004; Rogers and Johnson 2007; Svoma 2010). The availability of remotely sensed, reanalysis, and field campaign data has led to an increased understanding of gulf surges in recent years, providing insights into their kinematic and thermodynamic mean structure and their relationship to the monsoonal rainfall distribution (Gochis et al. 2004; Higgins and Gochis 2007; Johnson et al. 2007; Lang et al. 2007). Less understood remains their dynamics: while generally thought of as

*Corresponding author address*: Salvatore Pascale, California Institute of Technology, MC 131-24, 1200 E. California Blvd., Pasadena, CA 91125.
E-mail: spascale@gps.caltech.edu

DOI: 10.1175/MWR-D-15-0429.1

some type of coastally trapped disturbances (e.g., Zehnder 2004; Newman and Johnson 2012b, 2013), a specific dynamic definition is still lacking.

Recent work has clarified the relationship between GoC surges and larger-scale disturbances both in the tropics and the extratropics. Since the seminal studies by Stensrud et al. (1997) and Fuller and Stensrud (2000), it has been well known that at synoptic time scales (2–8 days) the initiation of a GoC surge is linked to the passage of a tropical easterly wave (TEW) trough or a tropical cyclone (TC) across southwestern Mexico (at around 20°N). The relationship between gulf surges and TEWs/TCs has been confirmed by subsequent studies (Anderson et al. 2000; Higgins et al. 2004; Higgins and Shi 2005; Bordoni and Stevens 2006; Schiffer and Nesbit 2012; Favors and Abatzoglou 2013; Seastrand et al. 2015). Among these, Higgins et al. (2004) emphasized how the extent to which a surge is followed by positive (wet surge) or negative (dry surge) precipitation anomalies over the southwestern United States cannot be discriminated based on the presence of TEWs. Rather, it is the position and the persistence of the upper-level anticyclone over the central and western United States that determines whether a surge is either wet or dry.

While these results suggest that synoptic-scale variability plays a dominant role in GoC surges, the summertime precipitation over AZWNM shows distinctive spectral peaks at frequencies lower than $1/8\,\mathrm{day}^{-1}$ (Nolin and Hall-McKim 2006), implying that other variability at longer time scales modulates the monsoonal flow, and possibly GoC surges. For instance, a quasi-biweekly (QBW) mode, likely associated with westward-propagating equatorial Rossby waves, is known to modulate precipitation over Central America, including southern Mexico (Kikuchi and Wang 2009; Jiang and Waliser 2009). On even longer time scales, Higgins and Shi (2001) show that the Madden–Julian oscillation (MJO) impacts the NAM precipitation through a meridional adjustment of the rainfall pattern over the eastern tropical Pacific. This adjustment leads to increased precipitation to the west of Mexico during the MJO westerly phase in the eastern Pacific. Lorenz and Hartmann (2006) extended these results by demonstrating that the westerly phase of the MJO is also positively correlated with precipitation over AZWNM. Further, the dynamical link is provided by the modulation of the TEWs/TCs by the MJO off the western coast of Mexico (e.g., Maloney and Hartmann 2000) that in turn trigger gulf surge development. Subtropical variability of NAM precipitation has also been linked to extratropical variability, primarily associated with extratropical Rossby wave trains (RWTs) propagating from the northwestern Pacific into North America (Kiladis and Hall-McKim 2004; Jiang and Lau 2009).

Despite the existing rich body of literature, a comprehensive understanding of how large-scale tropical and extratropical variability affects the GoC surges and associated precipitation patterns has yet to emerge. More specifically, no study that we are aware of has provided a systematic analysis of these links across temporal scales, spanning from synoptic to subseasonal, and across spatial scales, spanning from GoC to global scales. Such systematic analysis is the goal of this paper. In particular, we investigate the link between GoC surges, which are well known to provide the necessary lower-level moisture transport to support summertime convection over AZWNM, and tropical and extratropical modes of variability at different time scales. To do this, we use an improved GoC surge index based on principal component analyses of the near-surface winds along the GoC (Bordoni and Stevens 2006), and we identify large-scale patterns associated with GoC surge events. One key question we address is how and to what extent do these large-scale modes determine whether a surge results in wet or dry conditions over AZWNM.

Our methodology is similar to that of Wu et al. (2009) but, rather than focusing on regional patterns associated with lower-level moisture flux into the GoC, here we focus on global patterns related to GoC surges. Another important difference is that while their index is based on the lower-level moisture flux at one grid point at the southern entrance of the GoC, our index is based on coherent wind patterns along the entire GoC. We argue that our method has several advantages: 1) it more directly links GoC surges to modes of variability of the lower-level monsoonal circulation, 2) it allows for more direct associations with variability in the AZWNM precipitation, and 3) it can be directly extended to analysis of general circulation model (GCM) outputs, as it is based on dynamical variables rather than poorly simulated water variables (e.g., Liepert and Previdi 2012; Liepert and Lo 2013; Hasson et al. 2013).

In section 2, we give a brief overview of the datasets used in this study and describe our methodology in detail. The relationship between gulf surges and summertime AZWNM precipitation is analyzed in section 3. In section 4 we discuss how gulf surges are related to atmospheric tropical and extratropical waves at different time scales, while in section 5 we explore the impact of this variability on strong and weak precipitation events. A comparison with results from previous studies is provided in section 6. A summary follows in section 7.

## 2. Data and methodology

### a. Reanalysis and observational data

We use the 20 June–30 September 1979–2014 sea level pressure; 10-m wind; precipitation; 925-hPa specific humidity; vertically integrated moisture flux; and 700-, 500-, and 200-hPa geopotential height and wind from the European Centre for Medium-Range Weather Forecasts interim reanalysis product (ERA-Interim, hereafter ERA-I; Dee et al. 2011; Berrisford et al. 2011a). The atmospheric model on which ERA-I is based has 60 vertical levels and a horizontal resolution of about 79 km (Berrisford et al. 2011b), which allows for the GoC and the topographical features of the region to be sufficiently well resolved. While the results presented in this paper are based exclusively on ERA-I, we have verified that analyses based on the National Aeronautics and Space Administration Goddard Space Flight Center Modern-Era Retrospective Analysis for Research and Applications (MERRA; Rienecker et al. 2011), available from 1979 to 2010, are consistent with those reported below. As done in previous studies (e.g., Higgins et al. 1997), here we primarily focus on the influence of GoC surges on the precipitation over AZWNM, defined as the area between 31°–36°N and 114°–108°W. This target area does not include central and eastern New Mexico, as summertime precipitation in this region has been shown to be primarily influenced by upslope winds from the Great Plains (Lorenz and Hartmann 2006). To verify the realism of the reanalysis precipitation field over AZWNM, we have compared the ERA-I summertime daily precipitation with the NOAA/Climate Prediction Center (CPC) U.S. Unified Gauge-Based Analysis of Precipitation (Chen et al. 2008), with a horizontal resolution of 0.25° × 0.25° and daily time resolution (available online at http://www.esrl.noaa.gov/psd/data/gridded/data.unified.daily.conus.html).

### b. Principal component analysis of GoC surface winds

Although different definitions of GoC surges exist in the literature, qualitatively they are all based on metrics that identify the development of an intense southeasterly flow along the GoC. The index we use here is based on the 20 June–30 September 1979–2014 "alongshore" GoC wind $v_{\mathrm{gulf}}$, which is the component of the 10-m wind field parallel to the GoC axis, defined positive for northward flow and restricted over the GoC (Fig. 1a). The near-surface wind along the GoC is a good proxy for the vertically integrated moisture flux. In fact, the first principal components (PC1) of the near-surface wind and the vertically integrated moisture flux (Fig. 1a) are highly correlated (≈0.8). The choice of a wind-based index, rather than one based on moisture fluxes or precipitation data, is justified by the fact that wind is more readily accessible in observations (e.g., Bordoni et al. 2004) and more reliably simulated in reanalyses and GCMs than water variables (e.g., Liepert and Previdi 2012; Liepert and Lo 2013; Hasson et al. 2013).

To isolate synoptic, submonthly, and subseasonal atmospheric variability of the GoC and AZWNM region, daily means are obtained for all fields of interest from the 6-h ERA-I data. The seasonal cycle is then removed by applying a Lanczos high-pass filter (Duchon 1979) with a cutoff frequency of 120 days (e.g., Kikuchi and Wang 2009). Mean and linear trends are also removed from the time series for the period of interest (i.e., 20 June–30 September) [roughly corresponding to the onset and retreat of the NAM over AZWNM; Higgins et al. (1997)], so that all statistics are computed for anomalies relative to the summertime climatology. In the following, unless stated otherwise, we will always indicate alongshore GoC wind anomalies as $v_{\mathrm{gulf}}$.

Following Bordoni and Stevens (2006), we perform an EOF analysis based on the temporal unstandardized covariance matrix of $v_{\mathrm{gulf}}$. The first and second principal components (PC1 and PC2) account for 62% and 20% of the variance, respectively. The time series of PC1 is shown in Fig. 1a for one specific season (summer 2004). The spatial structure of the first EOF associated with PC1 represents a mode with strong, northward $v_{\mathrm{gulf}}$ over the whole GoC. In fact as discussed in Bordoni and Stevens (2006), PC1 is highly correlated (≈0.97) with the time series of the domain-averaged, $\langle\cdot\rangle$, alongshore wind anomalies (i.e., PC1 $\propto \langle v_{\mathrm{gulf}}\rangle$), thus allowing for a simple physical interpretation of PC1.

The power spectrum of PC1 reveals a rich structure of peaks at different frequencies (periods), suggesting that several dynamical processes, likely of tropical origin, might be at play in shaping the GoC wind variability. Specifically, three broad bands are noticeable: (i) several narrow peaks between 5 and 10 days, likely to be associated with the passage of TEWs or TCs south of the GoC entrance; (ii) a broader peak between 10 and 20 days, probably due to lower-frequency tropical modes (e.g., Jiang and Lau 2009; Kikuchi and Wang 2009); and (iii) a broad peak in the 30–90-day band likely to be associated with the MJO. The power spectrum of the leading PC of the vertically integrated alongshore moisture flux exhibits a similar structure and is also shown in Fig. 1b for comparison.

The approach of Bordoni and Stevens (2006)—who identified GoC surge events as days when the standardized PC1 is larger than 0.75 (i.e., 75% of its standard deviation)—captures GoC surges featuring strong, southerly wind anomalies along the entire gulf. However, in some cases GoC surges are associated with large,

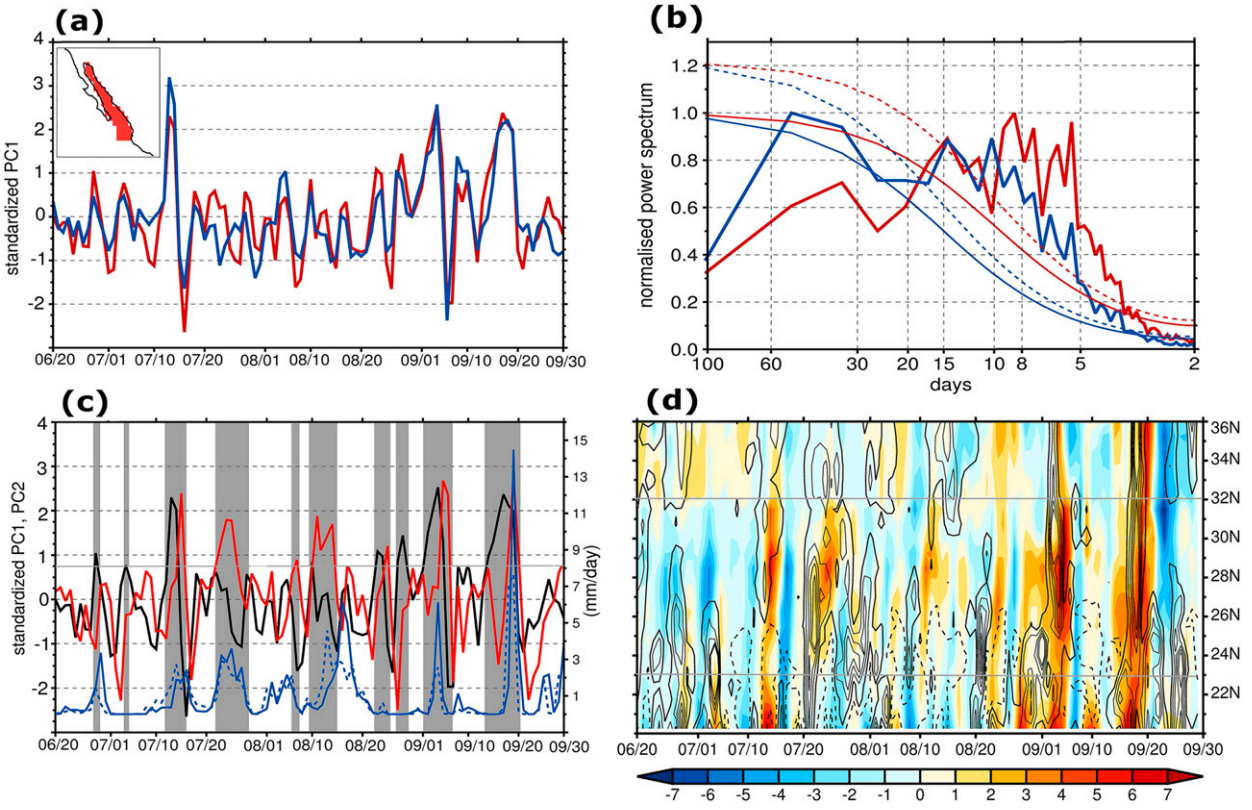


FIG. 1. (a) Standardized PC1 of the daily alongshore 10-m wind (red) and of the vertically integrated moisture flux (blue) anomalies over the GoC for the summer 2004 (the small box in the upper-left corner shows the GoC area used for the EOF analysis of the near-surface alongshore wind anomalies). (b) Normalized power spectrum, averaged over the period 1979–2014, of the PCs shown in (a). The smoothed curves are the red noise and the dashed lines are the 95% a priori confidence limit (Gilman et al. 1963). (c) Standardized PC1 (black) and PC2 (red) of the daily alongshore 10-m wind anomalies over the GoC, and AZWNM area-averaged daily precipitation (blue: ERA-I, dashed blue: CPC; see section 2a for the definition of the AZWNM region) for the same time period. Values of PC1 and/or PC2 greater than 0.75 (horizontal gray line) are associated with surge events. Surges identified with our method are highlighted with gray shading. (d) Hovmöller diagram of the alongshore 10-m wind anomalies over the GoC (shaded, units: m $s^{-1}$) and precipitation anomalies (contour, units: 2 mm $day^{-1}$; dashed: negative values) in a land strip along the eastern side of the GoC (south of 31.5°N) and over AZWNM (north of alongshore 10-m wind anomalies over the GoC). The two gray lines denote the latitude of the southern tip of Baja and the northern end of the GoC.

positive $v_{gulf}$ anomalies only in the northern part of the GoC, and close-to-zero or negative $v_{gulf}$ anomalies in the southern portion. Minor surges documented by Adams and Comrie (1997) belong to this category. To give a practical example, let us consider the summer 2004, a season accurately sampled and widely documented by the North American Monsoon Experiment observational campaign (Johnson et al. 2007; Higgins and Gochis 2007; Rogers and Johnson 2007). The Hovmöller (latitude–time) diagram of winds and precipitation (Fig. 1c) shows an example of such occurrences: on 22 July 2004 the GoC surge event, which led to more than 20 mm of rain over AZWNM, is characterized by $v_{gulf}$ positive and negative anomalies north and south of 25°N, respectively. Hence, this event is not captured by a surge index entirely based on PC1 (Fig. 1c).

To include these events, we extend our analysis to consideration of PC2, whose standardized time series is shown in Fig. 1c for summer 2004. The EOF2 associated with PC2 has a node at 25°N, with positive (negative) $v_{gulf}$ anomalies north (south) of this latitude. Therefore, large positive values of PC2 indicate a large north–south difference in GoC wind anomalies. The surge event on 22 July 2004 corresponds to a large value of PC2 (≈1.7). We find that PC2 is highly correlated (≈0.98) with the difference between the domain-averaged $v_{gulf}$ north and south of the node latitude 25°N (i.e., PC2 $\propto \langle v_{gulf}\rangle^{north} - \langle v_{gulf}\rangle^{south}$). This physical interpretation of PC2 is confirmed by a comparison of PC2 with $v_{gulf}$ anomalies (Figs. 1c and 1d).

By comparing PC1 and PC2 (e.g., Fig. 1c), it is evident that in most cases a large peak in PC1 (large $\langle v_{gulf}\rangle$) precedes a large peak in PC2 (large $\langle v_{gulf}\rangle^{north} - \langle v_{gulf}\rangle^{south}$) by about 1 day (e.g., see the surge event on 13 July 2004). The lag correlation between PC2 and PC1 indeed has

TABLE 1. Number of total surges (dry plus wet) for different thresholds in PC1 (PC2) used to identify surge events, and percentage of wet surges and (within brackets) their contribution to the total area-average 1979–2014 JJAS ERA-I precipitation over AZWNM (1.0 mm day$^{-1}$) for different values of the precipitation threshold used to define wet and dry surges.

| PC threshold | 0.5 | 0.65 | 0.75 | 0.85 | 1.0 | 1.5 |
|---|---|---|---|---|---|---|
| No. of surges | 737 | 704 | 673 | 623 | 548 | 293 |
| Precipitation threshold | | | | | | |
| 0.5 mm | 74% (85%) | 74% (79%) | 75% (76%) | 75% (70%) | 75% (60%) | 82% (37%) |
| 1.0 mm | 64% (84%) | 65% (78%) | 63% (73%) | 65% (69%) | 65% (59%) | 69% (36%) |
| 1.5 mm | 56% (82%) | 56% (76%) | 55% (72%) | 57% (67%) | 57% (58%) | 63% (36%) |
| 2.0 mm | 51% (81%) | 52% (75%) | 51% (71%) | 52% (66%) | 52% (57%) | 58% (35%) |
| 3.0 mm | 44% (79%) | 44% (73%) | 44% (68%) | 44% (64%) | 44% (55%) | 50% (34%) |
| 4.0 mm | 39% (76%) | 38% (69%) | 37% (65%) | 38% (61%) | 38% (53%) | 44% (32%) |
| 6.0 mm | 30% (70%) | 29% (63%) | 29% (60%) | 30% (56%) | 29% (48%) | 32% (29%) |

a maximum at lag −1. This sequence—large PC1 peak followed by a large PC2 peak—thus describes the life cycle of a major surge, which initially extends over the entire GoC and then, as the disturbance propagates farther north, persists just over the northern portion of the GoC (Fig. 1d). Although this is the most frequent case, other surge events, as the one on 22 July 2004, feature a large (>0.75) peak in PC2 preceded only by a modest (<0.75) peak in PC1. These are typical of less frequent, more localized GoC surges that either originate or strengthen in the middle of the GoC. Since here we are interested in assessing the overall contribution of all GoC surges to the NAM, we also include these events in our analysis.

### c. *Identifying GoC surges*

As discussed in section 2b, we use both PC1 and PC2 to extend the GoC surge definition of Bordoni and Stevens (2006) and also include surges that are localized in the GoC and correspond to large PC2 values only. The following algorithm is applied to identity the onset, duration, and end of each individual GoC surge:

1) For each year within the analysis period 1979–2014, we determine the days $t = \{t_1, t_2, \ldots, t_n\}$ for which *either* PC1 *or* PC2 is above a given threshold (e.g., 0.75); for example, if PC1 > 0.75 on 11 and 12 July and PC2 > 0.75 on 12 and 13 July, then 11–13 July satisfy this condition.
2) We then collect all surge days and group them by surge events, that is, $t = \{t_1^{(1)}, t_2^{(1)}, t_3^{(1)}, t_1^{(2)}, t_2^{(2)}, t_3^{(2)}, t_3^{(2)}, \ldots\}$. The last day of a surge event [e.g., $t_3^{(1)}$] and the onset of a successive one [e.g., $t_1^{(2)}$] have to be separated by at least one nonsurge day, for which PC1 *and* PC2 are both less than 0.75.
3) The onset day of an individual surge event $k$ is, therefore, $t_1^{(k)}$ and its end $t_m^{(k)}$ where $m$ is the number of days the $k$th GoC surge lasts. Figure 1c shows, for example, GoC surges that are identified with this method during summer 2004.

According to this procedure, we identify 673 GoC surges for the entire analysis period, corresponding to a mean of 18 surges per summer, which is equivalent to roughly 4 per month. This is in line with estimates obtained in previous studies using different methods (Bordoni and Stevens 2006; Fuller and Stensrud 2000; Higgins et al. 2004; Schiffer and Nesbit 2012). While the threshold in the gulf surge index chosen to identify individual surge events (0.75) is somewhat arbitrary, results with slightly different threshold values are not substantially different (Table 1). It is only for large threshold values (e.g., 1.5) that results differ substantially, with a sharp decrease in the number of identified surges.

## 3. GoC surges and precipitation over the southwestern United States

### a. *GoC surge flow and precipitation*

To develop an understanding of the average atmospheric patterns associated with GoC surges, we construct lagged regressions of atmospheric fields on our modified gulf surge index. Unlike in Bordoni and Stevens (2006), in this study in addition to lagged regressions on the standardized PC1, we also take into account lagged regressions onto PC2 in order to have a more complete view of all GoC surges. When adding lagged regression coefficients on PC2 to those on PC1, we shift regression fields on PC2 by 1 day (e.g., PC1-lagged regression at day 0 is added to PC2-lagged regression at day −1) since the lag correlation between PC2 and PC1 has a maximum at lag −1, that is, a peak in PC2 tends to follow by 1 day a peak in PC1 (e.g., Fig. 1c). While the inclusion of PC2 in the regression analysis does not affect substantially our results, regressions on PC2 are complementary to those on PC1 and provide a more complete description of patterns associated with GoC surge events.

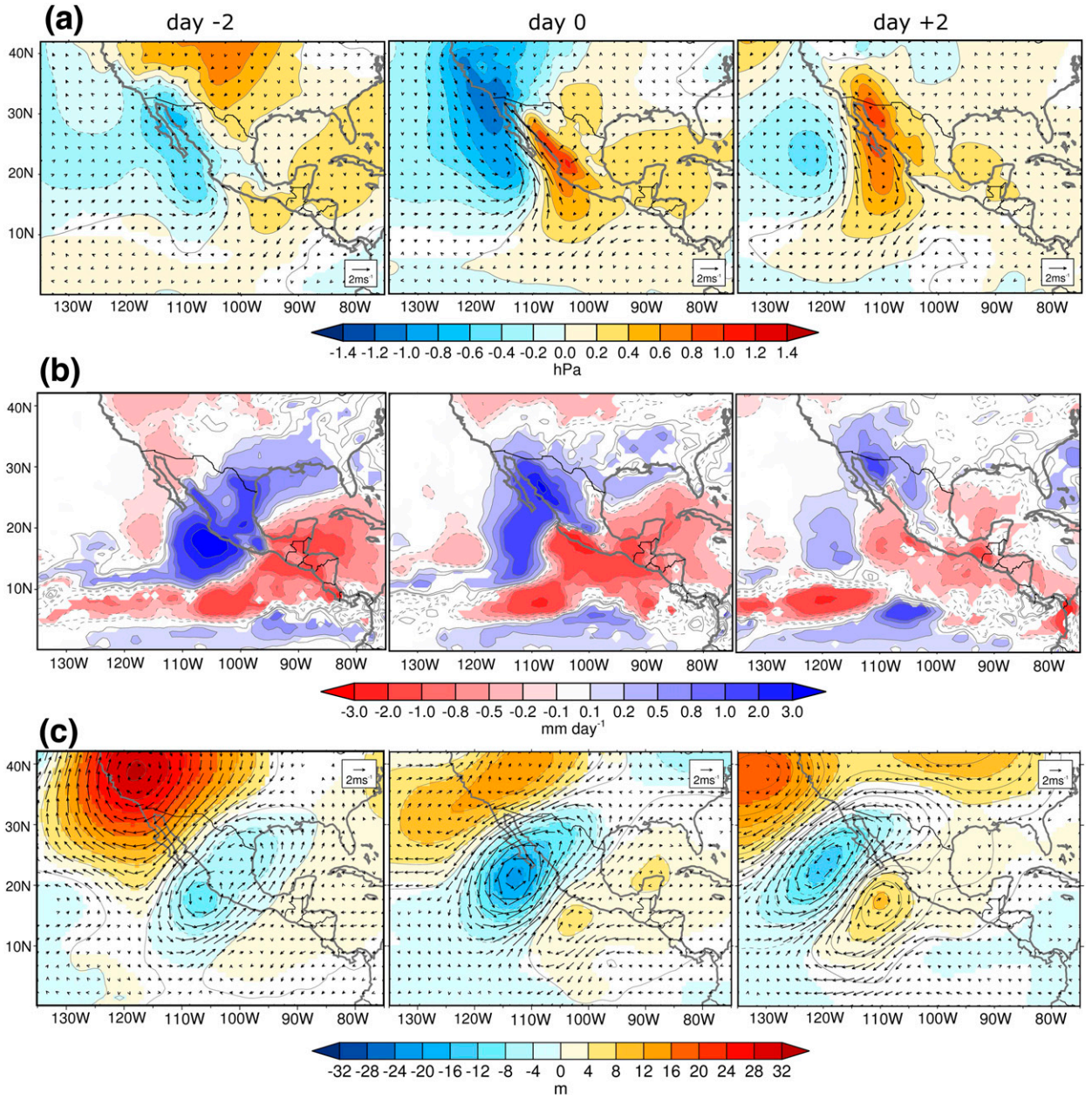


FIG. 2. Lagged regressions at day −2, 0, and +2 of (a) ERA-I 10-m wind and sea level pressure, (b) precipitation, and (c) 500-hPa wind and geopotential anomalies onto PC1 and PC2 (see text for details). Positive (negative) precipitation anomalies are solid (dashed). Shading indicates regions where anomalies are statistically significant at the 5% level.

The typical time evolution of a GoC surge is shown in Fig. 2 through lagged regressions of low-level wind, sea level pressure, precipitation, and 500-hPa wind and geopotential anomalies. Presurge atmospheric conditions (day −2) are characterized by a cyclonic anomaly developing over and south of the GoC due to a TEW or a TC passing across Central America. Northward wind anomalies larger than $1\,\mathrm{m\,s^{-1}}$ start developing south of the GoC entrance at 19°N. In the midtroposphere (Fig. 2c), we observe a cyclonic anomaly with two minima: a primary one to the south of the GoC and a secondary one over northeastern Mexico. While the deeper minimum is associated with a TC or a TEW reinforcing over the eastern Pacific, the secondary minimum is likely to be associated with an upper-level inverted trough (Pytlak et al. 2005; Bieda et al. 2009; Finch and Johnson 2010; Seastrand et al. 2015), which suggests that GoC surges can be further enhanced by these upper-tropospheric vorticity

anomalies (e.g., Newman and Johnson 2012a). At surge onset (day 0), southeasterly wind anomalies have propagated northward into the GoC and the cyclonic anomaly associated with the TEW/TC, located to the southwest of the tip of Baja Peninsula, has merged farther north with a midlatitude synoptic trough over the western United States. The positive pressure anomaly over western Mexico and negative anomaly over the head of the GoC shown in Fig. 2a at day 0 further enhance the mean JAS lower-level pressure difference. This pressure difference is associated with the thermal low over desert areas of Arizona and California and higher sea level pressure at the mouth of the Gulf owing to the development of a cloudy, showery air mass (Brenner 1974; Adams and Comrie 1997). Positive precipitation anomalies extend all the way from 10° to 30°N at about 115°W, over the whole GoC and the Sierra Madre Occidental, trespassing into southern Arizona. Two days after surge onset, southeasterly wind anomalies remain confined to the northern portion of the GoC and over Arizona, while anomalies have switched to northerly south of 27°N. The positive precipitation anomalies have moved farther northward into the southwestern United States up to 40°N and affect most of Arizona and western New Mexico. Overall, similar patterns have been found in previous studies in association with surge events in one specific summer season (Anderson et al. 2000; Berbery and Fox-Rabinovitz 2003; Gochis et al. 2004; Rogers and Johnson 2007), and in Douglas and Leal (2003) from radiosonde observations.

### b. *Contribution to AZWNM summertime precipitation*

While most studies have focused on average patterns associated with wet/dry surges, here we further quantify the precipitation–surge relationship using the surge index introduced in the previous section. As discussed in previous studies (e.g., Higgins et al. 2004; Schiffer and Nesbit 2012), not all GoC surges lead to enhanced precipitation in the southwestern United States because of unfavorable anticyclonic anomalies centered over the West Coast that tend to suppress the destabilization provided by the lower-level southerly GoC flow. The two surge events occurring between 20 August and 1 September 2004 (Figs. 1c,d) are examples of gulf surges that do not result in significant precipitation over AZWNM.

To distinguish a wet from a dry surge, the amount of rain accumulated during each event is calculated as the sum of daily precipitation during each surge event, as defined above. We include one additional day after the surge end day because, in most cases, precipitation in AZWNM tends to be delayed by 1 or 2 days with respect to the surge onset (Fig. 1c). If the accumulated rainfall exceeds a given threshold, the surge is defined as wet; otherwise, it is defined as dry. We adopt a threshold of 2 mm, which is roughly consistent with the mean ERA-I June–September (JJAS) rainfall rate over the AZWNM region (1 mm $day^{-1}$).

Figure 3a shows the scatterplot of total mean JJAS precipitation for each analysis year versus the number of total, wet, and dry surges. A robust positive correlation exists between the mean JJAS precipitation and the number of wet surges, while a robust negative correlation exists with the number of dry surges. Numbers of both wet and dry surges vary over a broad range (3–18). Interestingly, the number of all (wet and dry) surges shows a narrower interval, ranging from 13 to 22 and averaging at 18 surges per year. This number is largely consistent with the highest frequencies (periods between 6 and 9 days) of PC1 shown in Fig. 1a and most likely associated with TEWs/TCs. The number of wet and dry surges is instead consistent with a much wider range of frequencies (from 5–6 to 30 days or more), thus suggesting that atmospheric variability contributing to the NAM precipitation can greatly vary—from synoptic to subseasonal—from year to year, as suggested by Nolin and Hall-McKim (2006).

The number of wet surges within each summer has a direct control on the total JJAS rainfall. Figure 3b shows the mean JJAS precipitation, the number of wet surges and their rainfall contribution for the 1979–2014 period. The three time series are all positively correlated. On average, more than 70% of JJAS total precipitation over AZWNM is due to wet surges, with the remaining 30% due to non-surge precipitation events. These percentage values do not vary substantially if other PC or precipitation thresholds are chosen (Table 1). Most wet surges occur in July (≈3) and August (≈4) (Fig. 3c). These two months coincide with the mature phase of the NAM (Adams and Comrie 1997), during which about 60% of all surges are wet. When the whole JJAS period is taken into account, this percentage is lowered to 50%. Such findings are consistent with previous studies by Higgins et al. (2004) and Schiffer and Nesbit (2012), who estimated about 56% of July–August surges to be wet. Interestingly, we find that while September has fewer wet surges than July, their rainfall contributions are comparable, with a tendency for wet surge-related precipitation toward higher extremes (as shown by the whisker boxes in Fig. 3d). This is due to the fact that GoC surges in September are often associated with TCs moving northward close to or into the GoC (Higgins and Shi 2005; Corbosiero et al. 2009; Wood and Ritchie 2013).

## 4. Large-scale tropical and midlatitude controls of GoC surges

The role of TEWs and midlatitude upper-level disturbances in the initiation and evolution of GoC surges

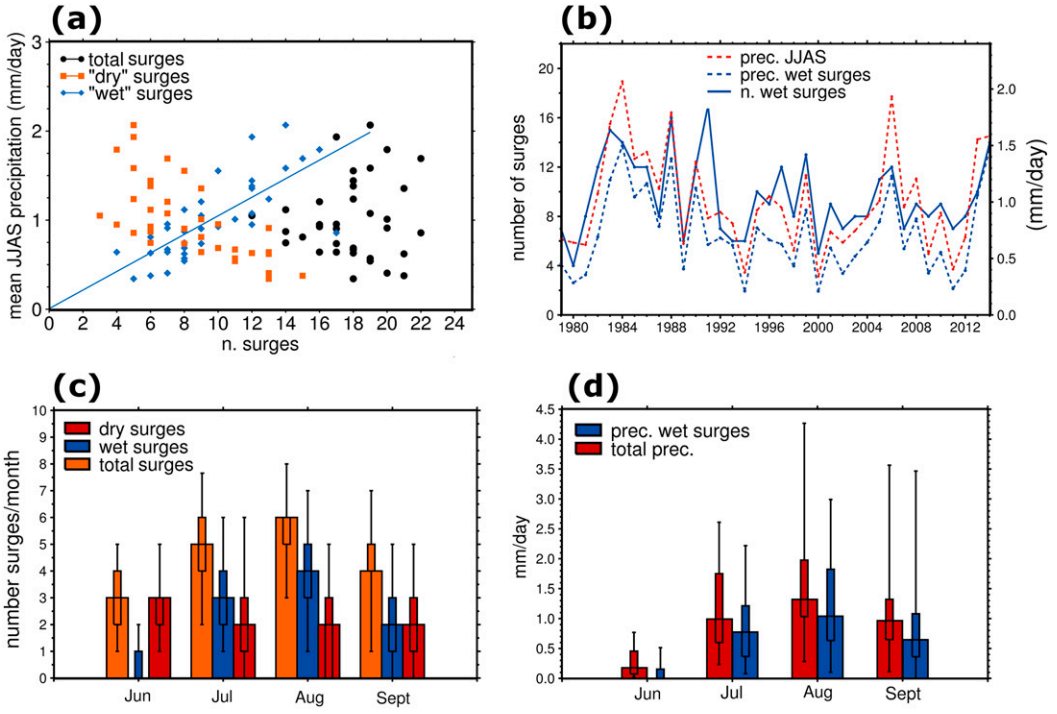


FIG. 3. (a) Scatterplot of JJAS precipitation averaged over AZWNM vs number of total, dry, and wet surges for each year of the analysis period (1979–2014). (b) Time series of annual JJAS AZWNM mean precipitation (red dashed line), JJAS mean AZWNM precipitation associated with wet surges (blue dashed line), and number of wet surges (solid blue line). (c) Seasonal distribution of the number of dry, wet, and total surges. Whisker plots show the minimum, 25th quantile, median, and 75th quantile and maximum. (d) As in (c), but for monthly AZWNM precipitation and monthly total AZWNM precipitation due to wet surges. A threshold of 2 mm is assumed here for discriminating between dry and wet surges.

has long been recognized in the literature (e.g., Stensrud et al. 1997). The relationship between surges and larger-scale disturbances in both the tropics and extratropics is also evident from the lagged regressions in Fig. 2. However, tropical and midlatitude disturbances vary on time scales ranging from synoptic to submonthly and subseasonal. This variability in turn influences the variability in the GoC winds, as evidenced in the PC1 spectrum (Fig. 1b). Hence, to disentangle the role of disturbances at different time scales on the GoC surges, in the following we repeat the regression analysis of the previous section on PC1 and PC2 after filtering the fields of interest within the three broad time windows (2–8, 10–20, and 25–90 days) suggested by the PC1 spectrum (Fig. 1b). Unlike most previous studies, we do not limit our analysis to the North American region, but extend it to most of the Northern Hemisphere, to infer large-scale signals of nearly global impact.

### *a. Synoptic variability: 2–8 days*

GoC wind variability in the 2–8-day band is dominated by TEWs/TCs. The TEW/TC signal in the southwestern Mexican region just before a GoC surge event is evident in the regression maps of sea level pressure, precipitation, wind, and the 700-hPa geopotential height anomaly shown in Figs. 4 and 5. The interaction between a TEW and the orography of Central America creates a cyclonic anomaly downstream of the topography (Fig. 4a), at times developing into a TC, which then propagates along the Mexican coastline and leads to northward winds along the GoC (e.g., Zehnder 1991; Zehnder et al. 1999; Serra et al. 2010). This mode, which explains the series of peaks in the power spectrum of GoC mean $v_{gulf}$ (Fig. 1c), has a period of nearly 6 days: consistently, the southerly flow (day 0) along the GoC (Fig. 4a) is reversed after about 3 days. In tandem with the TEW/TC progression pattern, precipitation and 925-hPa specific humidity anomalies (Figs. 4b,c) intensify over the western coast of Central America just south of the GoC. The positive precipitation and humidity anomalies then further strengthen over the Sierra Madre Occidental (day 0) to finally spread northward into the southwestern United States, where wet conditions remain confined to southern Arizona and persist for no more than 2 days. The shape of

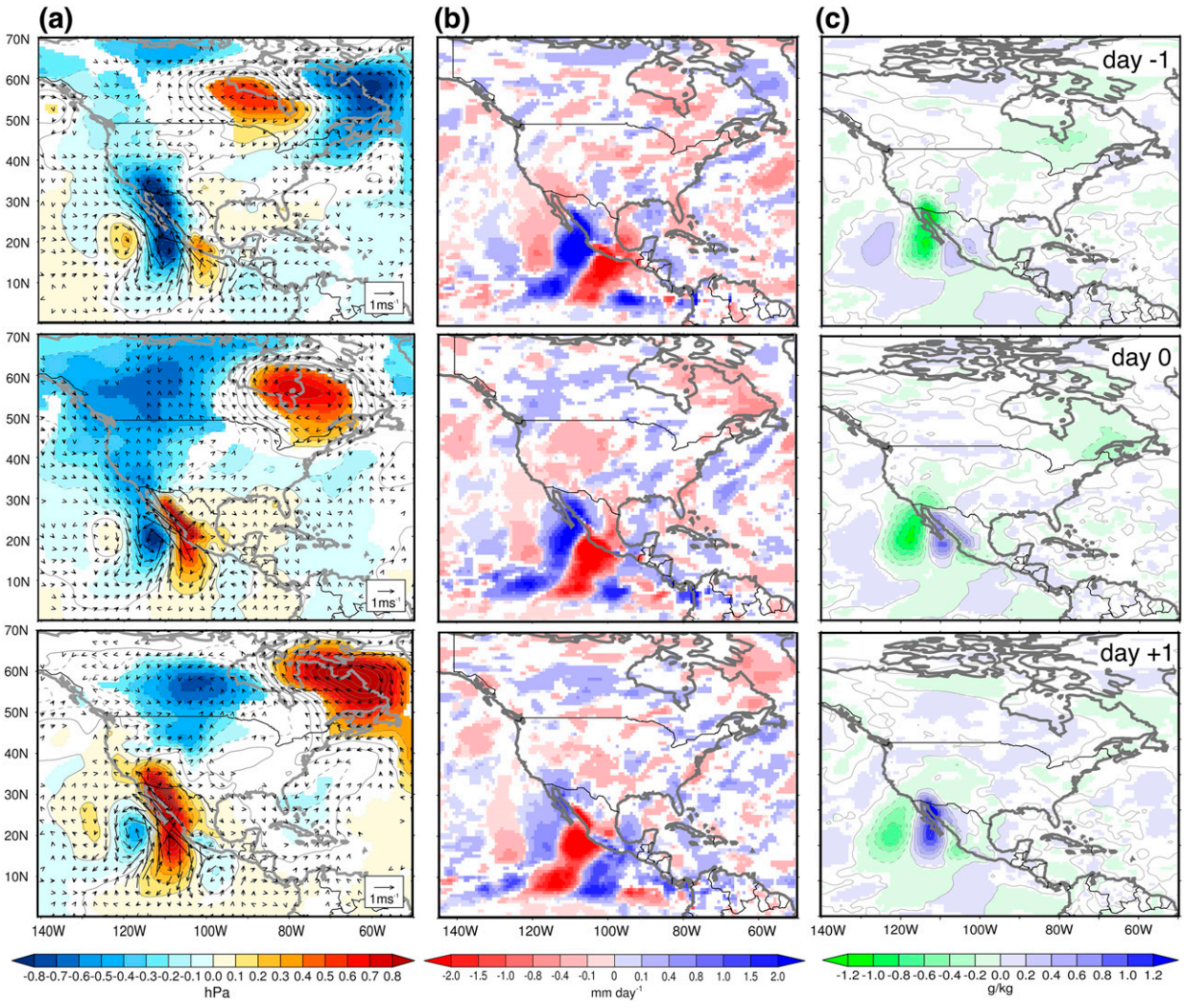


FIG. 4. Lagged regressions of the ERA-I 2–8-day filtered (a) mean sea level pressure and 10-m wind, (b) precipitation, and (c) 925-hPa specific humidity anomalies. Vector fields and color shading are shown only where significant at the 5% level.

near-surface anomalies associated with the development of a surge event raises the question as to what extent these patterns are dominated by strong TCs. Especially later in the monsoon season, TCs can develop over the tropical eastern Pacific and move northward with tracks to the west of Baja California, and, in fewer cases, even inside the GoC. To adress this question, we repeat our analyses 1) excluding September months and 2) identifying and excluding from our analysis all days in the 1979–2014 period during which a TC[1] tracked north of 15°N. The resulting patterns (not shown) do not reveal major differences with the ones that include TCs. More specifically, when TCs are excluded, the wavelike 10-m wind and sea level pressure anomaly patterns to the south of the GoC (Fig. 4) are displaced southward by a few degrees, and feature a weaker and less circular cyclonic anomaly. Resulting patterns of alongshore wind, moisture, and precipitation in the monsoon region, however, remain largely unchanged (not shown).

Figure 5 shows lagged regressions of 200- and 700-hPa wind and geopotential height. In addition to the sequence of disturbances associated with the TEWs/TCs, clearly visible at 700 hPa (Fig. 5b), a midlatitude trough passes over the western United States at day 0 at all vertical levels (Figs. 4a and 5). This trough is embedded within a stream of circumglobal, eastward-propagating Rossby waves (e.g., Chang and Yu 1999; Chang 1999) and favors a moist, southerly flow into the southwestern

[1] We used the National Hurricane Center best track data available online at http://www.nhc.noaa.gov.

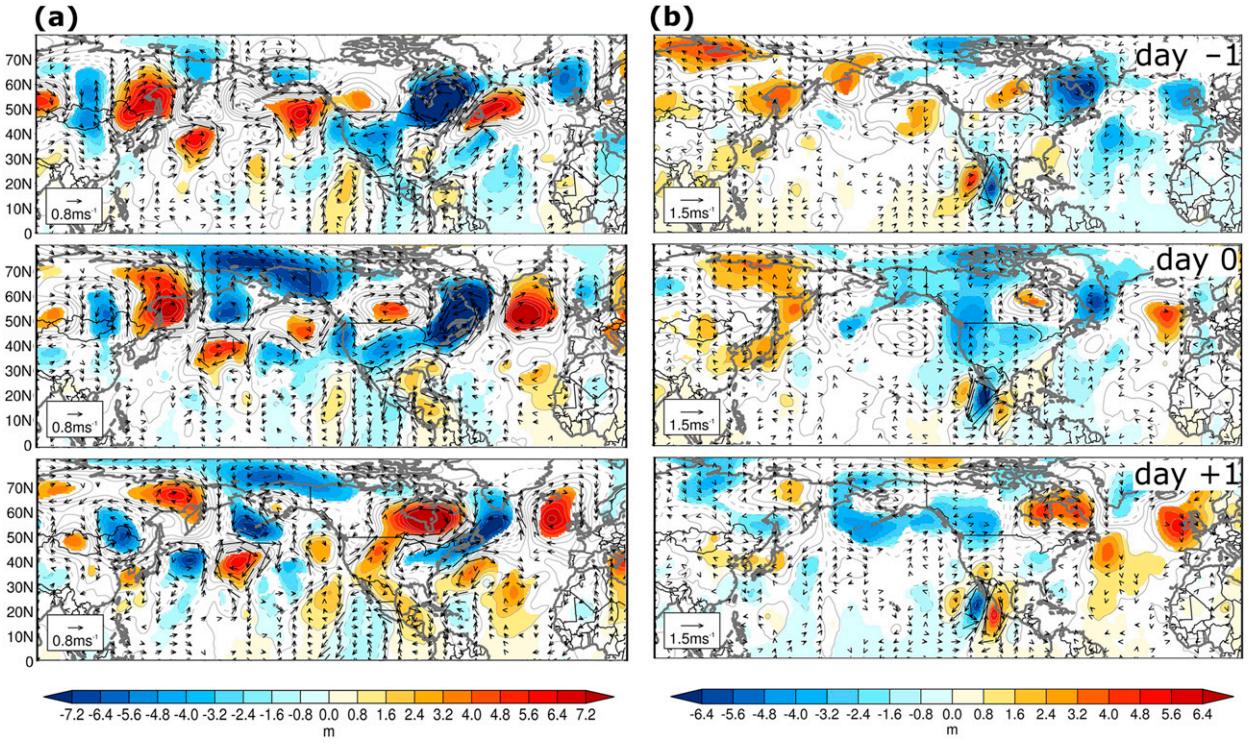


FIG. 5. Lagged regressions of the ERA-I 2–8-day filtered geopotential height and wind at (a) 200 and (b) 700 hPa. Vector fields and color shading are shown only where significant at the 5% level.

United States at the lower levels (day 0, +1) and an easterly flow at the upper levels from the Gulf of Mexico (day +2). The phasing between the TEW and the midlatitude trough is more concisely illustrated by the Hovmöller diagrams in Figs. 6a and 6b, showing the regressed meridional wind anomalies in the tropics (15°N, to capture the TEWs) and at midlatitudes (45°N, to capture the Rossby waves). The progression of eastward Rossby waves is more pronounced in the upper atmosphere (200 hPa), but it is in the lower–midatmosphere (700 hPa) that the interaction between tropical and extratropical waves is more evident. In the days following the onset of the surge event, when precipitation in the AZWNM region is anomalously high (day +1), positive anomalies simultaneously occur at about 110°W at both tropical and midlatitudes, indicating that the synchronization between the two waves supports the development of a southerly flow from the GoC into the southwestern United States.

At the synoptic time scale, upper-level inverted troughs have also been argued to enhance mesoscale convective activity over the Sierra Madre Occidental (e.g., Pytlak et al. 2005; Finch and Johnson 2010). The resulting convective outflows as they propagate westward toward the GoC can result in minor moisture surges extending only over the northern GoC. Given that these minor surges are captured by PC2, it is reasonable to expect that wind regressions on PC2 might reveal signatures of these inverted troughs (see section 2b). In Fig. 7 we show the 2–8-day filtered 200-hPa wind and geopotential anomalies regressed on PC2 only. The TCs have also been removed in order to better isolate upper-level inverted troughs, but note that including TCs reveals very similar and only slightly weaker patterns (not shown). The regressions in Fig. 7 clearly reveal that minor surges are usually associated with an upper-level trough, which strengthens over central Mexico at ~22°N at day −2 from the surge onset, and then propagates toward the GoC (day 0). The trough shape and trajectory are consistent with the track density climatology shown by Bieda et al. (2009). While the link between PC2 and these upper-level inverted troughs deserves more attention and will be the topic of a future investigation, these results highlight how our wind-based PC analyses not only allow for a characterization of large-scale patterns associated with all surges, but also allow us to distinguish between major and minor surges, and associated triggering mechanisms.

### b. *Quasi-biweekly variability: 10–20 days*

Lagged regressions in this time window emphasize a cyclonic structure, in proximity of the Baja Peninsula, which has a larger spatial extent than that seen in the

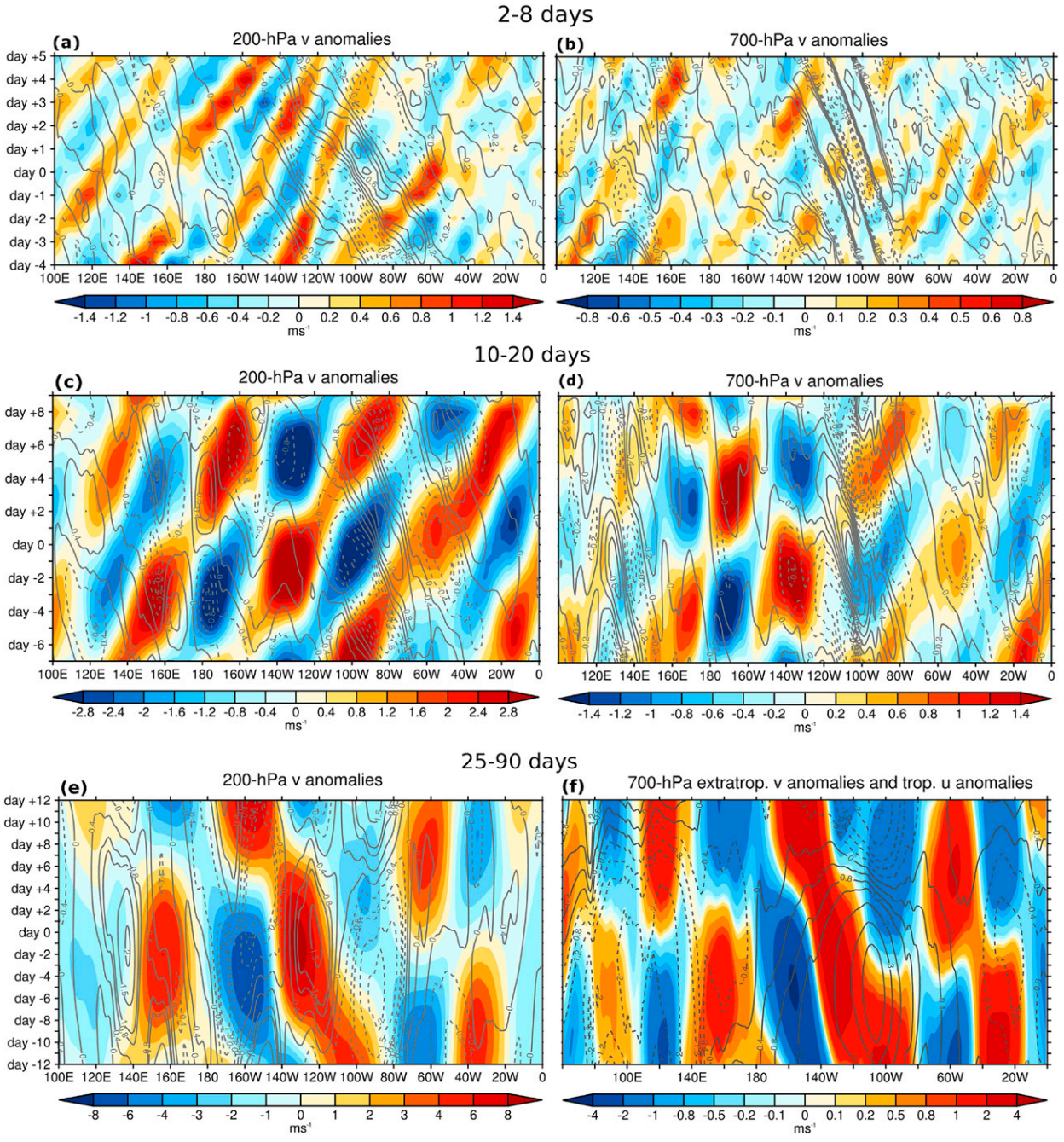


FIG. 6. (a),(b) Hovmöller longitude–time diagram of the 200- and 700-hPa 2–8-day filtered meridional wind anomalies averaged between a narrow midlatitude strip (45°–50°N, shaded) and tropical (10°–15°N, contour) latitude strip. (c),(d) As in (a),(b), but for 10–20-day filtered data. (e) As in (c), but for 25–90-day filtered data. (f) The 700-hPa 25–90-day filtered meridional wind anomalies averaged between a narrow midlatitude strip (45°–50°N, shaded) and zonal wind anomalies averaged around 13°N (10°–15°N, contour).

2–8-day case and a periodicity of about 18 days (Fig. 8a). Positive lagged regressions of precipitation and 925-hPa specific humidity anomalies over the southwestern United States last for 4–5 days, after which the positive pattern is stretched eastward into central and eastern United States (Figs. 8b,c). A negative correlation in precipitation and moisture anomalies exists in this time window between the southwestern and eastern United States. These patterns are consistent with those of Mullen et al. (1998), who found a spectral peak within the 12–18-day band when analyzing the Arizona summertime precipitation.

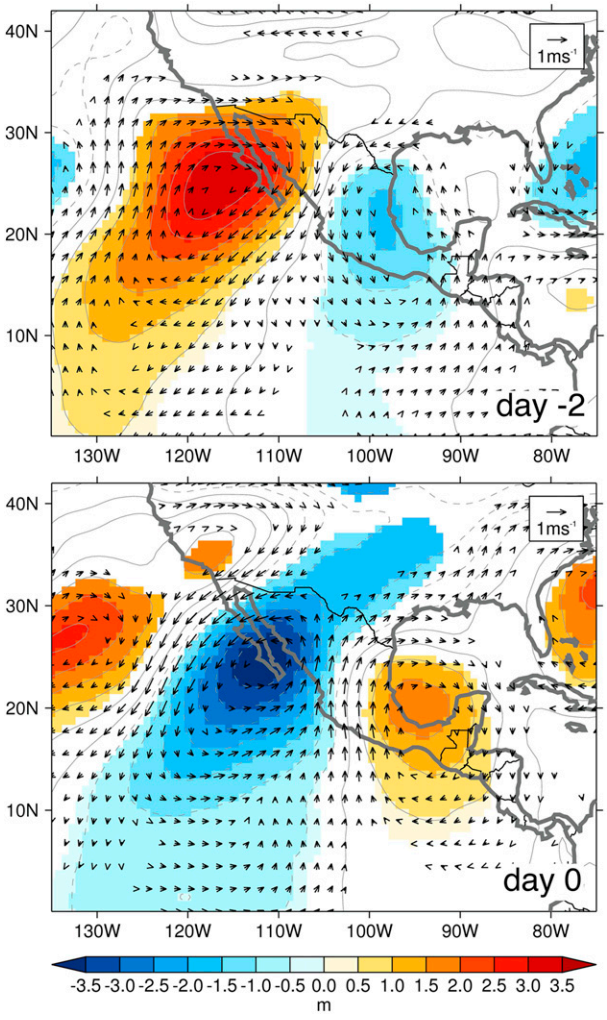


FIG. 7. Lagged regressions of the ERA-I 2–8-day filtered 200-hPa geopotential height and wind on PC2. Vector fields and color shading are shown only where significant at the 5% level.

Regressions of geopotential height and winds at 200 and 700 hPa (Fig. 9) reveal that the wet phase over the southwestern United States (from day +2 to day +6) is associated with the phasing between a midlatitude cyclonic anomaly, embedded within an RWT at about 50°N coming from the northwestern Pacific, and a tropical easterly disturbance propagating over Central America (QBW; e.g., see Kikuchi and Wang 2009). At 700 hPa, wind anomalies veer from northeasterly to southwesterly as the tropical trough and ridges advance westward and phase with the midlatitude cyclonic anomaly after day +2 (Fig. 9b). In the upper atmosphere (200 hPa), the wet phase (from day +1 to day +4) is sustained by southeasterly wind anomalies flowing along the eastern flank of the tropical and extratropical cyclonic centers, which are aligned along the 120° meridian at day +6 (Fig. 9a). This is consistent with the fact that the anomalous precipitation patterns over AZWNM in the 10–20-day band are sustained by moisture originating from the Pacific Ocean at lower levels and from the Gulf of Mexico at mid- to upper levels.

The progression and relative phasing of the tropical and extratropical wave packets at 200 and 700 hPa are summarized by the Hovmöller diagrams in Figs. 6c and 6d. While moving at about 5° day$^{-1}$ over the Atlantic and central eastern United States, the extratropical Rossby waves tend to be more standing over the Pacific and western United States. Note that the extratropical Rossby waves are essentially barotropic; the tropical waves associated with the QBW over Central America—and in the longitudinal band 140°–60°W—have instead a baroclinic structure, with sign inversion between the upper and lower level. This seems to be consistent with their interpretation as equatorial Rossby waves (Chatterjee and Goswami 2004; Kiladis et al. 2009).

### c. *Subseasonal variability: 25–90 days*

The regression maps in the 25–90-day time window emphasize patterns typical of the MJO evolution over the tropical Pacific Ocean: westerly and easterly phases in the surface winds, accompanied by dry and wet phases in precipitation over southeastern Asia and the eastern tropical Pacific, with a periodicity of about 50 days (Fig. 10). A GoC surgelike circulation develops and intensifies at the surface after the peak of the MJO westerly phase (day −4 to day +4), when a cyclonic anomaly develops west of the Baja Peninsula. A wet anomaly, previously located over the southeastern Pacific, shifts northward and reaches AZWNM at day −2, in association with a cyclonic anomaly in the lower to midatmosphere south of the GoC (Figs. 11b,c). As the MJO easterly phase intensifies (from day +4 onward), the surgelike circulation moves farther north and weakens, disappearing at day +8. However, the northwestward shift toward Alaska of the upper-tropospheric geopotential height previously centered over the western United States (Fig. 11a) enables the development of a cyclonic anomaly, which strengthens and moves its center over California by day +12, leading to southeasterly and then southerly anomalous flow into southwestern and central United States and allowing the wet anomaly to farther spread into these regions. Such a shift, corresponding to the arrival of a subsequent wave train, is evident from the Hovmöller diagram in Figs. 6e and 6f.

The positive geopotential height anomaly centered over the western United States (day −4 to day 0) is embedded within a low-frequency RWT. The centers of cyclonic and anticyclonic anomalies roughly form an

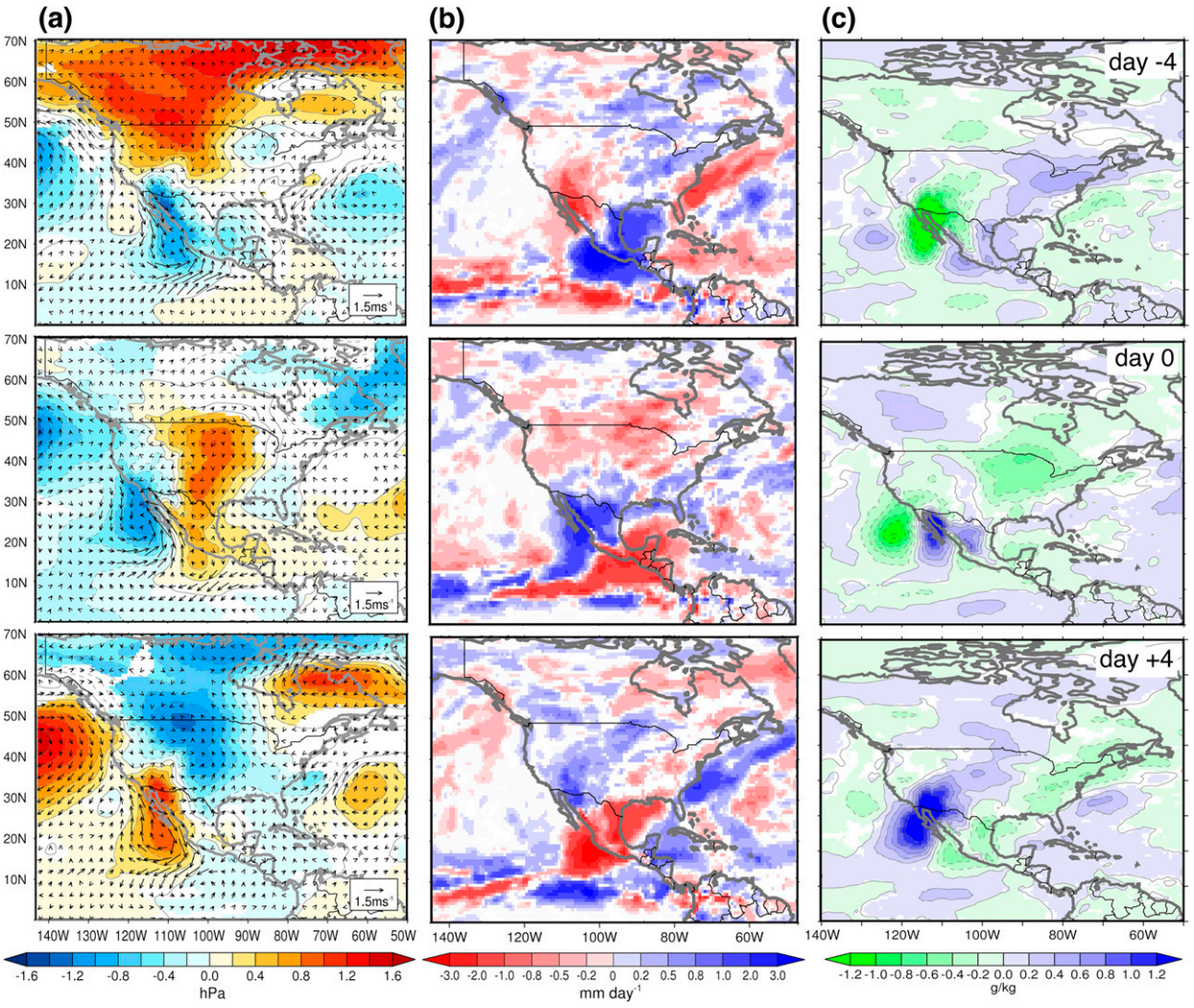


FIG. 8. As in Fig. 4, but with a 10–20-day filter has been applied to the data.

arch along the coast of eastern Asia and western North America (e.g., at day 0, Fig. 11). Contrary to the suggestion by Wu et al. (2009), this wave train seems to have a remote origin over the western Pacific rather than being a local response to the heating associated with precipitation anomalies in the eastern Pacific. Furthermore, comparison of the 200- and 700-hPa levels clarifies the double origin of such wave train: in the mid- to lower troposphere, one wave train originates from the western tropical Pacific, where it may be caused by heating associated with the precipitation anomaly in the Asian monsoon region; in the upper atmosphere, the other wave train has a straighter trajectory and comes from central Asia. The lower-level wave train first propagates upward and then merges with the upper-level wave train over the northwestern Pacific (Jiang and Lau 2009).

## 5. Intense and weak precipitation events associated with GoC surges

The results discussed so far describe average patterns associated with all surges, with no differentiation between wet and dry surges. Here, we investigate if and to what extent distinctive patterns in larger-scale waves can help discriminate between surges that result in weak or strong precipitation anomalies over AZWNM. To do so, we divide GoC surges identified in section 3b into ''dry'' and ''wet'' based on the AZWNM accumulated precipitation following the surge event: if the accumulated precipitation is less (more) than 0.5 mm (4 mm) the surge is classified as dry (wet). These thresholds correspond to a quarter and twice the mean spatially averaged accumulated AZWNM rainfall (≈2 mm) during 2 days. Based on this criterion, 132 surges are identified as dry, and 234 as

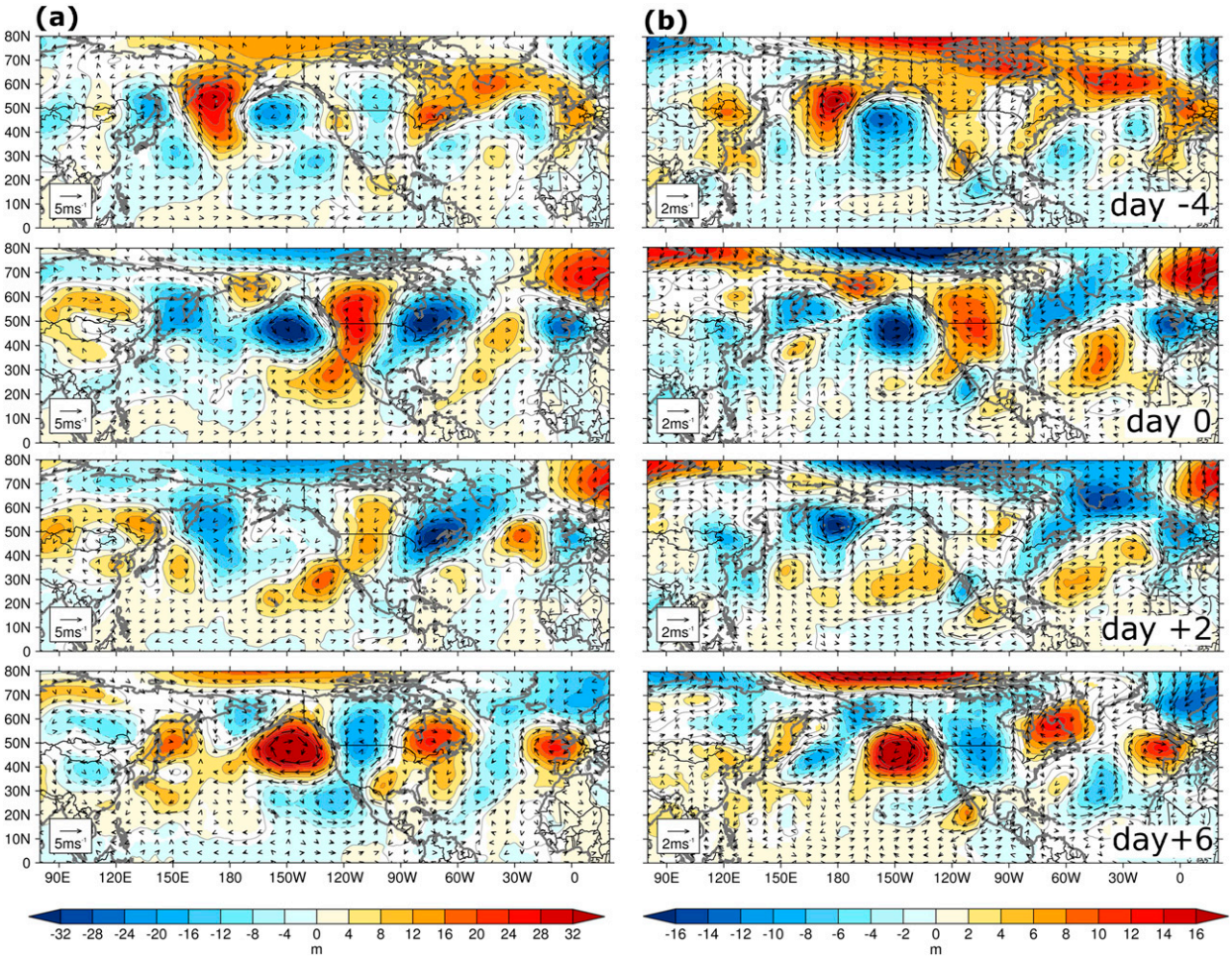


FIG. 9. As in Fig. 5, but with a 10–20-day filter has been applied to the data.

wet. Corresponding lagged regressions are then computed taking into account only ±6 days before and after the surge onset.

### *a. Link to 2–8-day variability*

On the 2–8-day time scale, wet and dry surges differ mainly in the position of the mid- to upper-tropospheric anticyclonic anomaly and of the TEW/TC signal (Fig. 12). At 200 hPa, we note that, in the wet surge case (Fig. 12b), a midlatitude trough embedded in a trans-Pacific eastward-propagating RWT moves over the western United States and, at day +2, is centered over the Rockies. This RWT also leads to an eastward shift over central United States of the anticylonic anomaly previously located over the Rockies. For dry surges, this Rossby wave pattern is much less evident at day +2, and the anticyclonic anomaly remains farther to the south over the NAM region (Fig. 12a).

This difference is even more evident at 700 hPa, where during wet surges the high pressure anomaly center is over the U.S. West Coast, while during dry surges it is located over the southwestern United States (day +2, Figs. 12c,d). The latter is a configuration that enhances anticyclonic conditions over AZWNM and favors northerly anomalous flow into the region, thus inhibiting convection.

At 700 hPa, we also note that in the wet surge case the circulation anomalies associated with TEWs/TCs are displaced northward by a few degrees relative to the dry surge case, in agreement with Schiffer and Nesbit (2012). This may be partially due to TCs that pass to the south of, or within, the GoC, and that are often associated with very intense GoC surge events (Johnson et al. 2007).

### *b. Link to 10–20-day variability*

Unlike what we see on the synoptic time scale described above, regression patterns associated with dry and wet surges differ substantially in the 10–20-day time window (Fig. 13). For dry surges, waves propagate along an arch-shaped trans-Pacific path connecting circulation

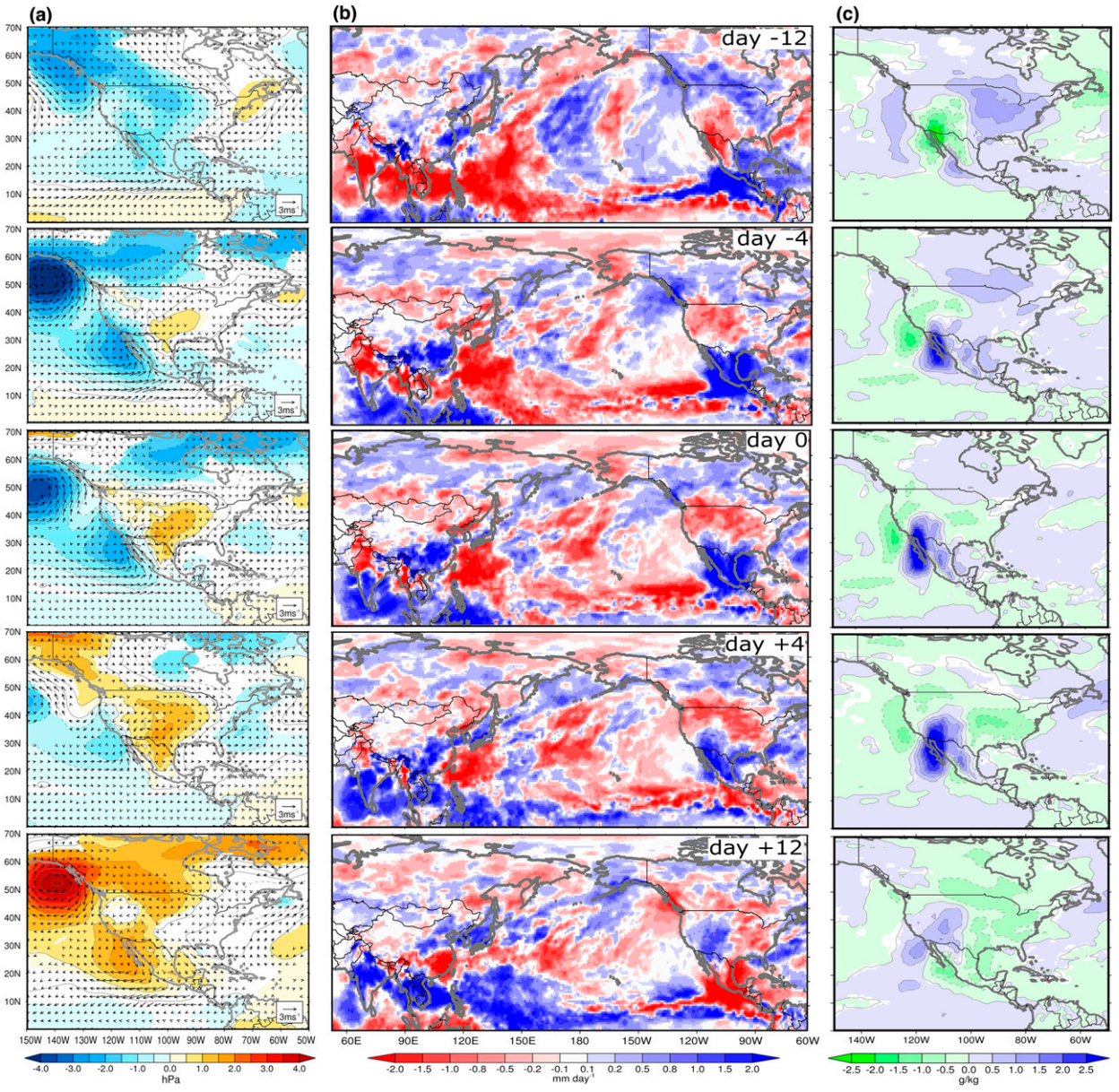


FIG. 10. As in Fig. 8, but with a 25–90-day filter has been applied to the data.

centers over the western Pacific with those over the eastern subtropical Pacific/North America. The wave train does not cross the eastern United States into the Atlantic basin. A cyclonic anomaly is found in the lower troposphere over the GoC (from day 0 to +4, Figs. 13c,d), which causes moist air to move over northwestern Mexico. However, no phasing is evident between the lower-level tropical and the upper-level extratropical troughs (Figs. 13c,d). In other words, dry surges are not accompanied by mid- to upper-level southeasterly flow bringing into the region moisture originating from the Gulf of Mexico.

Patterns associated with wet surges are substantially different than those associated with dry surges, in that the extratropical wave trains travel on a straighter eastward trajectory and penetrate into northern America reaching the Atlantic Ocean. This allows for a phasing between a tropical and extratropical trough (from day +3 to day +8), which supports the intrusion of moist air from the Gulf of Mexico in the upper troposphere (Figs. 13a, b; 200 hPa) and from the GoC in the lower troposphere (Figs. 13c,d; 700 hPa), into the southwestern and then central and eastern United States. These results, therefore, suggest that it is the extratropical variability in the

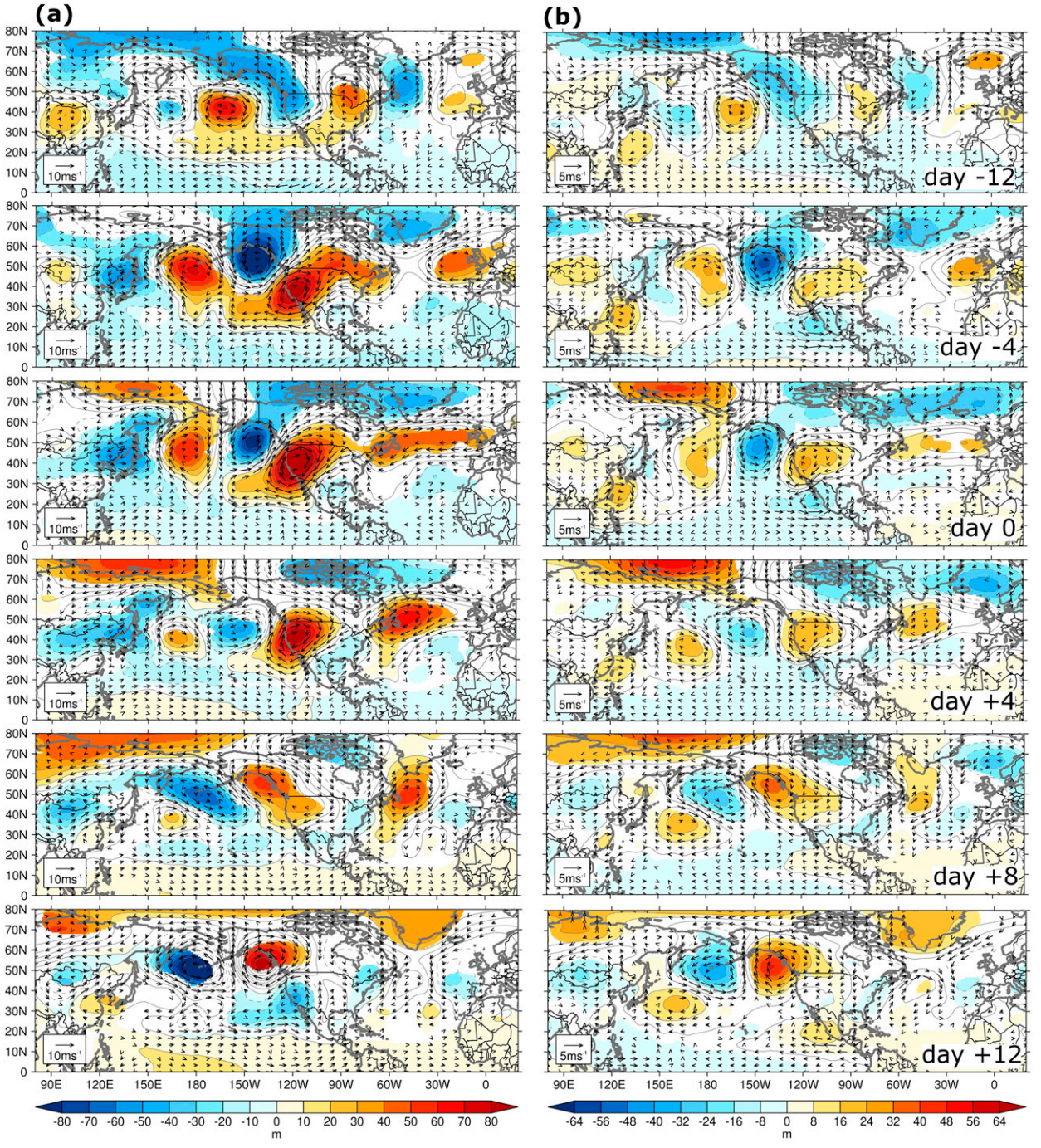


FIG. 11. As in Fig. 9, but with a 25–90-day filter has been applied to the data.

10–20-day frequency band that determines the degree of wetness and the northward extent of a surge.

### c. *Link to 25–90-day variability*

In the 25–90-day time window, wet and dry cases show different anomalous precipitation patterns over the United States (e.g., Fig. 10b; day +4 to day +12). Dry cases are accompanied by anomalies with smaller spatial extent and displaced farther eastward than wet cases (not shown), which explains the weaker rainfall over AZWNM. Such differences can be related to the different position of the cyclonic and anticyclonic anomalies associated with the

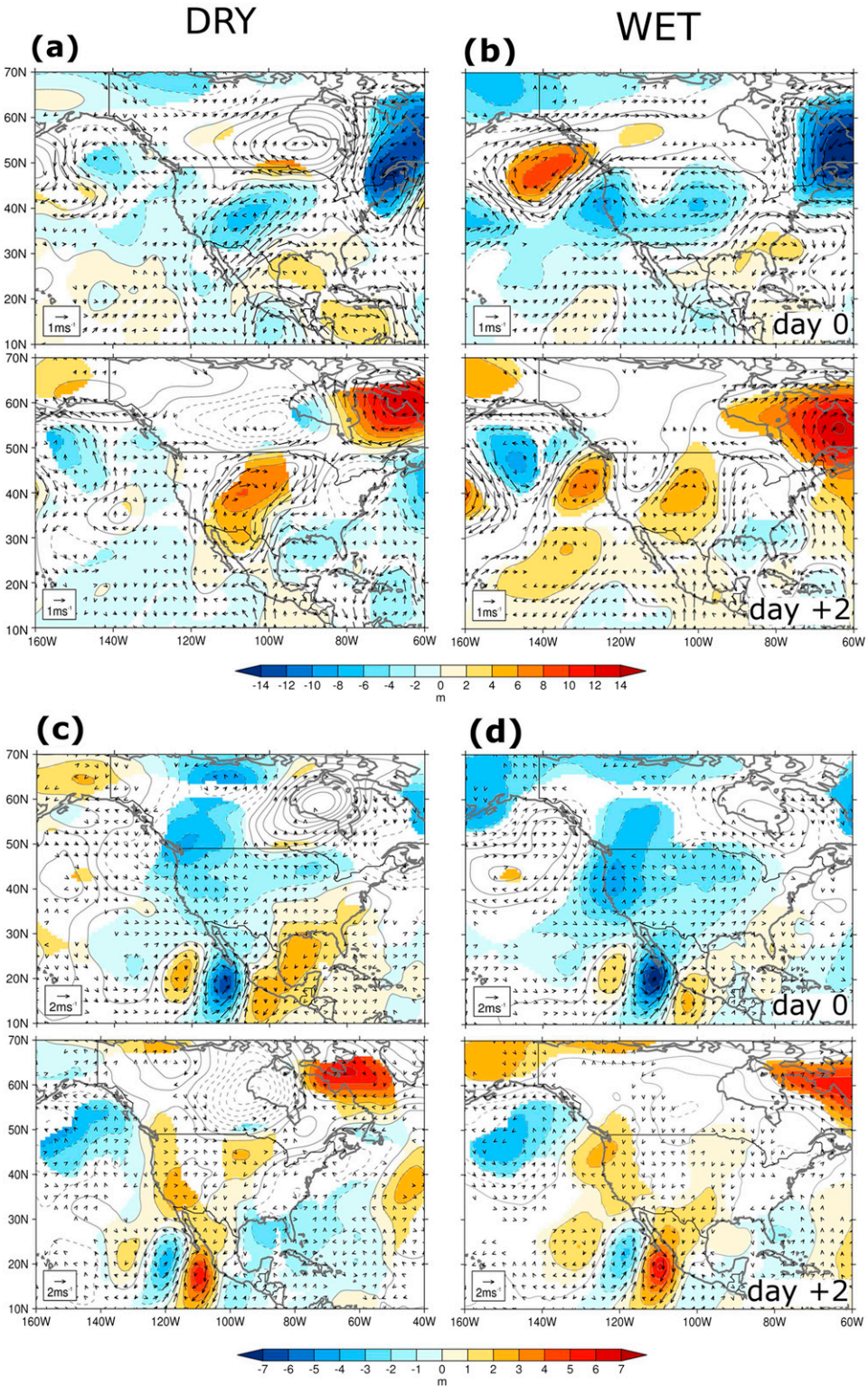


FIG. 12. Lagged regressions of 2–8-day filtered geopotential height and wind at (a),(b) 200 and (c),(d) 700 hPa for (left) dry and (right) very wet events over AZWNM. Please see text for dry/wet definitions. Vector fields and color shading are shown only where significant at the 5% level.

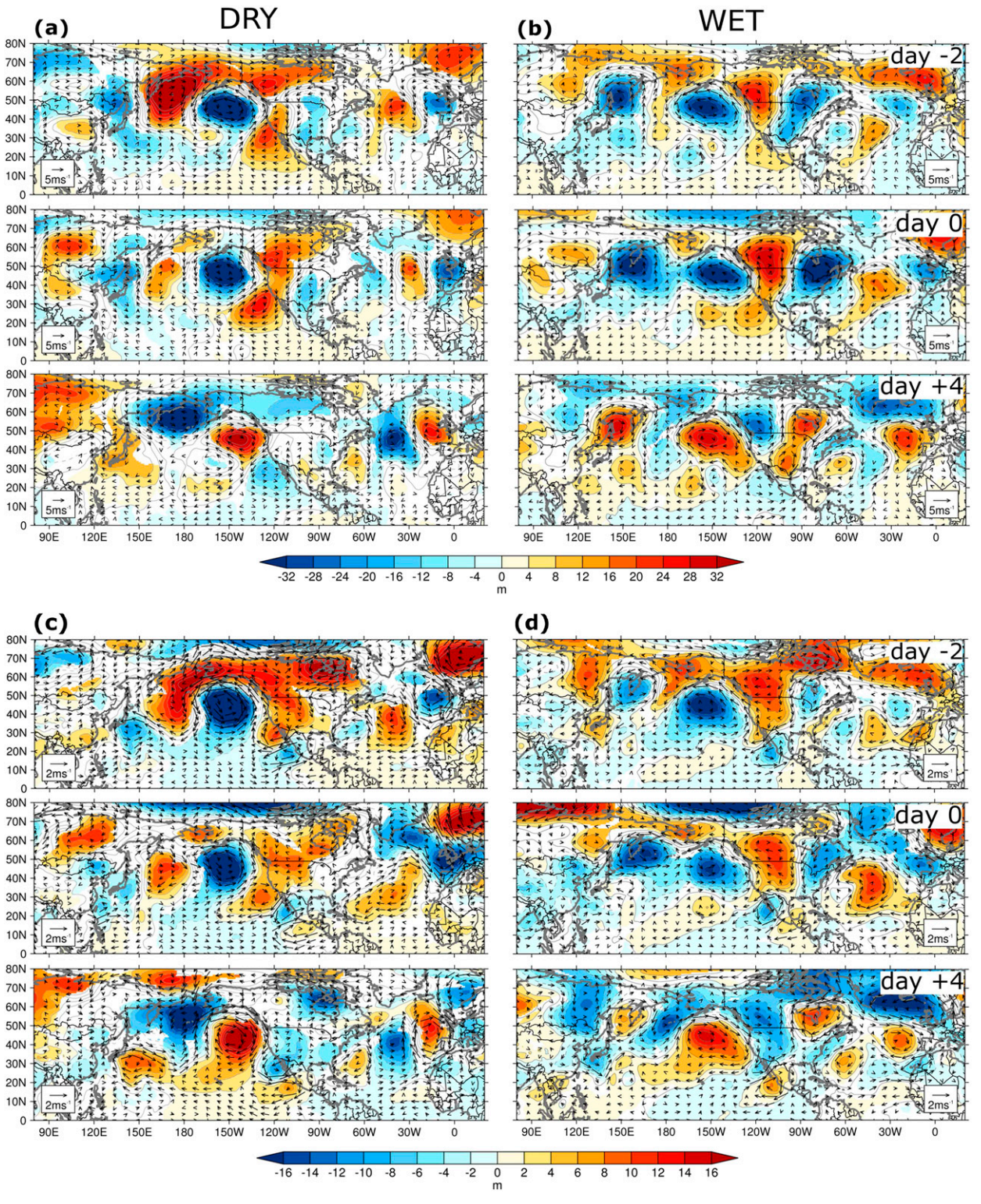


FIG. 13. Lagged regressions of 10–20-day filtered geopotential height and wind at (a),(b) 200 and (c),(d) 700 hPa for (left) dry and (right) very wet events over AZWNM. Vector fields and color shading are shown only where significant at the 5% level.

trans-Pacific RWT shown in Fig. 11. Before the spreading of wet anomalies into the southwestern and central United States (from day −4 to day 0), a positive geopotential height anomaly exists over the western North America, preventing the tropical cyclonic anomaly to the west of Mexico to move northward (Figs. 10 and 11). This anticyclonic anomaly is part of an arch-shaped RWT most likely generated at midlevels (Fig. 11b) by diabatic heating anomalies in the Asian monsoon region (Kawamura et al. 1996). This wave train then interacts and reshapes the upper-level RWT coming from central Asia (Jiang and Lau 2009), causing it to converge over western North America where it further strengthens the anomalous high. The arrival of a second energy impulse at about day +8 reshapes the trajectory of the RWT, suddenly shifting it northwestward and thus repositioning the anomalous high south of Alaska. It is this rearrangement of the wave patterns that then allows the tropical cyclonic anomaly west of Baja Peninsula to migrate into the western United States together with large amounts of rain (Fig. 10b; day +12).

The sequence of events we have just described is also seen in wet cases (Figs. 14b,d). The switch in the MJO polarity from westerly to easterly further reinforces the anticyclonic anomaly west of Mexico at about 15°N, which helps to direct moist air into northwestern Mexico and the southwestern United States. In the dry case, the rearrangement of the troughs and ridges somewhat differs from the phenomenology we have just described in that the anomalous high persists over central-western United States, preventing the tropical low associated with the western MJO phase to move northward (Fig. 14a). This, together with an incoming anomalous high appearing after the MJO phase switch to the west of Mexico (day 6), leads to the suppression of the GoC anomalous low and of convective activity over AZWNM. We are not aware at this time of mechanisms that might be responsible for these different fluctuations of the RWTs and their synchronization with the MJO. Further investigation is left for future work.

## 6. Discussion and comparison with previous studies

In this section, we provide a comparison between results emerging from our analyses, and those that have been previously reported in the literature. Some of the patterns discussed in this study are in fact in agreement with previous studies. Unlike previous studies, however, we have attempted to take a comprehensive approach based on variability of the low-level GoC flow that does not focus on one specific time scale. In this respect, this approach allows us to put previously highlighted results in a broader context.

On synoptic time scales, we find that GoC wind variability results in positive precipitation anomalies extending into western Mexico and the southernmost part of Arizona. The spatial pattern and duration (1–2 days) of these precipitation anomalies are consistent with the passage of a TEW/TC to the south of Baja Peninsula in the presence of a strong monsoon midlevel ridge, and they are in agreement with Seastrand et al. (2015), who found a similar pattern performing an EOF analysis of summertime precipitation anomalies over the NAM region. In agreement with previous studies (Schiffer and Nesbit 2012), we find that surges leading to strong or weak AZWNM precipitation differ mainly in terms of the position of the TEW/TC track and the mid- to upper-level trough–ridge over central and western United States at this time scale. Hence, our results suggest that while necessary to trigger gulf surges, TEWs/TCs are not a sufficient large-scale ingredient for enhanced precipitation events over AZWNM, with the midlatitude playing an important role as well (Higgins et al. 2004). Furthermore, regressions onto the second principal component of the alongshore wind (PC2) isolate the contribution of upper-level inverted troughs in the development of minor surges (Pytlak et al. 2005; Bieda et al. 2009; Finch and Johnson 2010; Newman and Johnson 2012a).

Variability at longer time scales (>10 days) must then play a major role. We have shown that in the 10–20-day frequency band wet surges are usually associated with an eastward-propagating extratropical ridge over the United States that is in phase with tropical QBW modes (Kikuchi and Wang 2009) passing over western Mexico (Fig. 9). At longer time scales (25–90 days), waves tend to propagate westward over the eastern Pacific (i.e., Fig. 6f), and wet conditions over AZWNM are related to a northwestward shift toward Alaska of the anomalous anticyclonic anomaly over western United States occurring during the reorganization of the Pacific wave train (Fig. 14). These observations help explain the finding of Higgins et al. (2004), who showed that wet surges occur when the midlevel anticyclonic anomaly sitting over the United States stretches longitudinally, leading to two maxima: the first one migrates westward from the western United States to Alaska, and the second one migrates eastward over the central eastern United States, thus favoring the influx of moist southeasterly air in the AZWNM region.

Previous work based on filtered precipitation data over AZWNM reveals similar patterns (e.g., Kiladis and Hall-McKim 2004; Jiang and Lau 2009). While these studies used different filters [i.e., an 8-day low-pass filter in Jiang and Lau (2009), a 30-day high-pass filter in Kiladis and Hall-McKim (2004)], the use of a precipitation-based

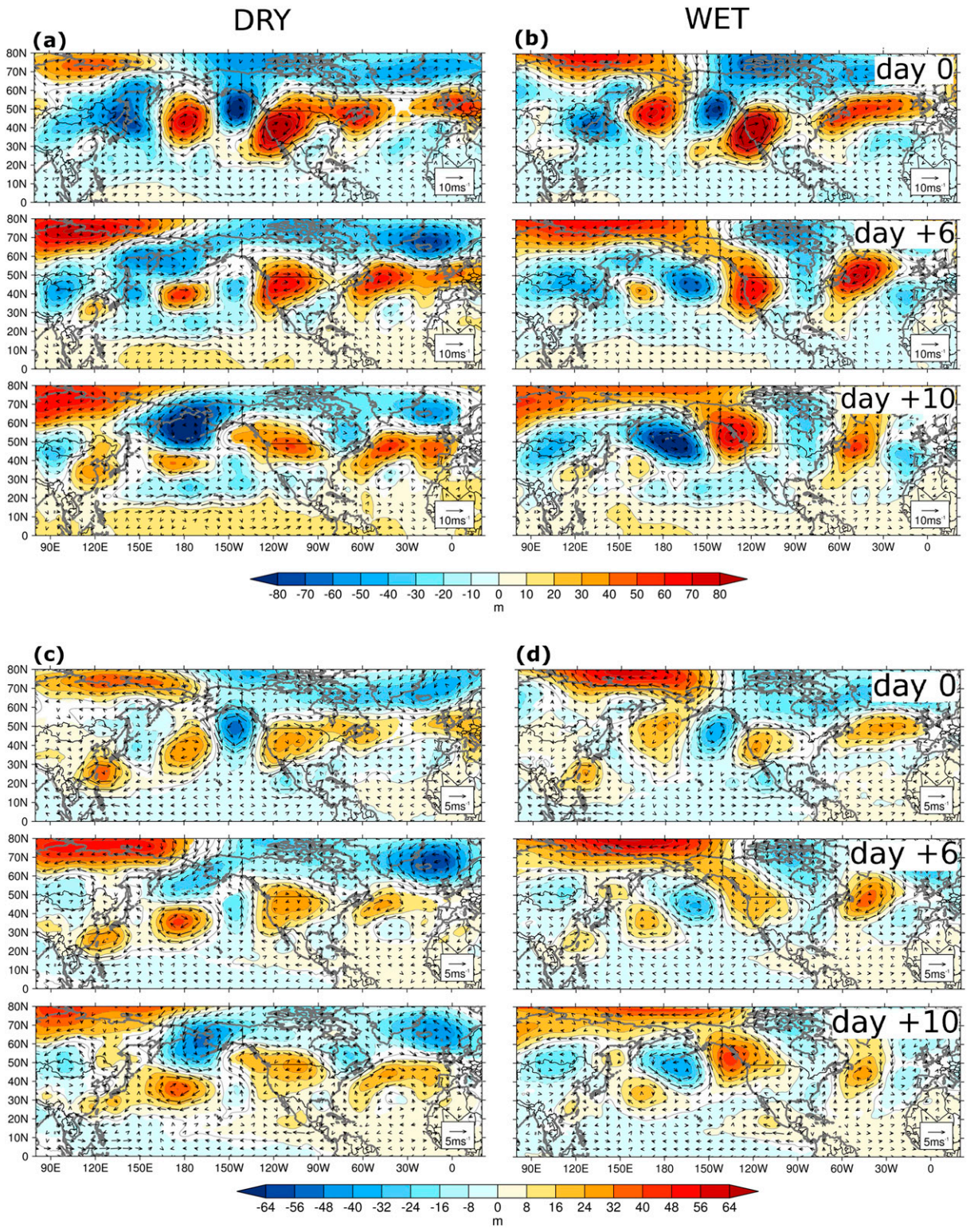


FIG. 14. Lagged regressions of 25–90-day filtered geopotential height and wind at (a),(b) 200 and (c),(d) 700 hPa for (left) dry and (right) very wet events over AZWNM. Vector fields and color shading are shown only where significant at the 5% level.

index inevitably emphasizes the 15–25-day frequency band, at which precipitation spectra broadly peak (Mullen et al. 1998; Mo 2000; Cavazos et al. 2002). Note that this band is somewhat intermediate between the two lower-frequency bands used in this paper.

The possible influence of the MJO on the AZWNM precipitation remains debated in the literature, with some studies claiming only a weak influence (e.g., Higgins and Shi 2001; Mo and Nogues-Paegle 2005) and others showing evidence of a modulation by the MJO, through modulation of GoC-surge-triggering TEWs and TCs (Lorenz and Hartmann 2006; Wu et al. 2009). Maloney and Hartmann (2000) showed that the low-level westerly (easterly) phase of the MJO over the eastern Pacific favors (disfavors) tropical cyclogenesis because it is accompanied by cyclonic (anticyclonic) low-level relative vorticity anomalies and near-zero (enhanced) vertical wind shear. This, in turn, may lead to strong GoC surges as, for example, in August–September 2004 (Johnson et al. 2007). Our results do suggest a modulation of the AZWNM precipitation by the MJO, through the development of cyclonic anomalies to the west of the Mexican coast, which are accompanied by surgelike southerly wind anomalies along the GoC. However, while the MJO has a more direct impact on the tropical NAM region, precipitation over the AZWNM region is also significantly impacted by mid-latitude waves, primarily through a trans-Pacific extratropical wave train connecting southeastern Asia with the eastern Pacific. This is likely to be tied to MJO-related convective activity over the Philippines at time scales of nearly 45 days (Kawamura et al. 1996), but a better understanding of these interconnections requires further research. Our results are at odds with the work of Jiang and Lau (2009), who suggest that the MJO has a negligible influence on the intraseasonal variabiliy of the NAM precipitation. This discrepancy might, however, be reconciled considering that previous studies using precipitation indices have emphasized the 15–25-day component (Mullen et al. 1998; Mo 2000; Cavazos et al. 2002); therefore, preventing a clear identification of the MJO signal. Here, we separate these time scales based on the low-level GoC wind spectrum, which helps to isolate better the MJO contribution to the NAM precipitation and circulation variability. More work is, however, needed to better elucidate these links, which we defer to future investigations.

## 7. Conclusions

In this study the connection between GoC surges and the larger-scale flow within and outside the NAM domain is explored by means of a surge index based on principal component analyses of the near-surface GoC winds. Links between this mode of variability and the summertime precipitation over the monsoon domain, with a specific focus on its northernmost extremity over Arizona and western New Mexico, are also explored. Our analysis is somewhat complementary to that by Wu et al. (2009), but it takes a more global approach in studying larger-scale dynamic controls on gulf surges, and at more comprehensively examining their relationship to the AZWNM precipitation at different time scales. The improved index introduced in this work is able to capture both major and minor surge events, which differ in their spatial extent along the GoC. We find that GoC surges contribute to roughly 70%–80% of the summertime mean rainfall over AZWNM and that the total summertime mean rainfall in this region is positively correlated with the number of wet surges during each monsoon season.

Regression analyses provide a coherent and complete picture of dynamical controls of GoC surges at the synoptic (2–8 days), quasi-biweekly (10–20 days), and subseasonal (25–90 days) time scales. We find that surgelike circulations can develop over the GoC in association with an upper-level inverted trough or from the interaction of TEWs/TCs with fast westerly Rossby waves on synoptic time scales, from the interaction of equatorial Rossby waves (QBW mode) with slower westerly Rossby waves at higher latitudes on quasi-biweekly time scales, and from the interaction of the MJO with quasi-stationary Rossby waves originating over southeast Asia on longer intraseasonal time scales. As expected, the positive precipitation anomalies associated with these surgelike circulations differ substantially in terms of duration of their spatial extent.

The relationship between GoC surges and intense/weak precipitation events over AZWNM is further explored at each time scale, which allows us to elucidate the time scales responsible for heavy/scarce rainfall. It is found that strong precipitation events occur primarily on time scales longer than synoptic, with the quasi-biweekly and subseasonal modes playing a dominant role in the development of these more extreme events. In particular the tropical–extratropical wave interaction at the 10–20-day time scale is a major player: surges developing without an adequate phasing between the trans-Pacific Rossby waves and the tropical QBW modes are scarce in precipitation over the southwestern United States.

While this study highlights the role that atmospheric variability on different time scales plays on the variability of the monsoonal circulation and precipitation, it still remains to be investigated how these different processes interact with each other. Moreover, in spite of

the many efforts to understand GoC surge variability at the subseasonal and smaller time scales, only a few studies have focused on surge variability on interannual time scales (e.g., Higgins and Shi 2001), which remains another fascinating field open to future research.

Comprehensive GCMs, such as those of phase 5 of the Coupled Model Intercomparison Project (CMIP5) archive (e.g., Taylor et al. 2012), project changes in the intensity and seasonality of NAM rainfall under increasing anthropogenic forcing (e.g., Cook and Seager 2013; Lee and Wang 2014; Pascale et al. 2016). As the NAM appears as an envelope of transient activity, characterizing the large-scale dynamical controls on this activity both in observations and in GCMs is the first necessary step to more robustly assess model performances and better constrain their future projections. Future work will employ high-resolution (≤50 km) GCMs (e.g., Delworth et al. 2012; Vecchi et al. 2014), capable of resolving the GoC, to investigate how gulf surges will be affected by changes in large-scale circulations due to global warming.

*Acknowledgments.* S. P. was supported by the NOAA Climate and Global Change Postdoctoral Fellowship Program, administered by the University Corporation for Atmospheric Research. We thank G. Kiladis for illuminating discussions on tropical waves, K. Kikuchi for providing code for estimating the statistical significance of spectral peaks, N. Feldl and two anonymous reviewers for their constructive comments on the first version of this manuscript.

## REFERENCES

Adams, D. K., and A. C. Comrie, 1997: The North American monsoon. *Bull. Amer. Meteor. Soc.*, **78**, 2197–2213, doi:10.1175/1520-0477(1997)078<2197:TNAM>2.0.CO;2.

Anderson, B. T., J. O. Roads, and S.-C. Chen, 2000: Large-scale forcing of summertime monsoon surges over the Gulf of California and the southwestern United States. *J. Geophys. Res.*, **105**, 24 455–24 467, doi:10.1029/2000JD900337.

Berbery, E. H., and M. S. Fox-Rabinovitz, 2003: Multiscale diagnosis of the North American monsoon system using a variable-resolution GCM. *J. Climate*, **16**, 1929–1947, doi:10.1175/1520-0442(2003)016<1929:MDOTNA>2.0.CO;2.

Berrisford, P., P. Kallberg, S. Kobayashi, D. Dee, S. Uppala, A. J. Simmons, P. Poli, and H. Sato, 2011a: Atmospheric conservation properties in ERA-Interim. *Quart. J. Roy. Meteor. Soc.*, **137**, 1381–1399, doi:10.1002/qj.864.

——, and Coauthors, 2011b: The ERA-Interim archive, version 2.0. ERA Rep. Series 1. Tech. Rep. ECMWF, 23 pp. [Available online at http://www.ecmwf.int/en/elibrary/8174-era-interim-archive-version-20.]

Bieda, S. W., C. L. Castro, S. L. Mullen, A. C. Comrie, and E. Pytlak, 2009: The relationship of transient upper-level troughs to variability of the North American monsoon system. *J. Climate*, **22**, 4213–4227, doi:10.1175/2009JCLI2487.1.

Bordoni, S., and B. Stevens, 2006: Principal component analysis of the summertime winds over the Gulf of California: A Gulf Surge index. *Mon. Wea. Rev.*, **134**, 3395–3414, doi:10.1175/MWR3253.1.

——, P. E. Ciesielski, R. H. Johnson, B. D. McNoldy, and B. Stevens, 2004: The low-level circulation of the North American monsoon as revealed by QuikSCAT. *Geophys. Res. Lett.*, **31**, L10109, doi:10.1029/2004GL020009.

Brenner, I. S., 1974: A surge of maritime tropical air—Gulf of California to the southwestern United States. *Mon. Wea. Rev.*, **102**, 375–389, doi:10.1175/1520-0493(1974)102<0375:ASOMTA>2.0.CO;2.

Cavazos, T., A. C. Comrie, and D. M. Liverman, 2002: Intraseasonal variability associated with wet monsoons in southeast Arizona. *J. Climate*, **15**, 2477–2490, doi:10.1175/1520-0442(2002)015<2477:IVAWWM>2.0.CO;2.

Chang, E. K. M., 1999: Characteristics of wave packets in the upper troposphere. Part II: Seasonal and hemispheric variations. *J. Atmos. Sci.*, **56**, 1729–1747, doi:10.1175/1520-0469(1999)056<1729:COWPIT>2.0.CO;2.

——, and D. B. Yu, 1999: Characteristics of wave packets in the upper troposphere. Part I: Northern Hemisphere winter. *J. Atmos. Sci.*, **56**, 1708–1728, doi:10.1175/1520-0469(1999)056<1708:COWPIT>2.0.CO;2.

Chatterjee, P., and B. N. Goswami, 2004: Structure, genesis and scale selection of the tropical quasi-biweekly mode. *Quart. J. Roy. Meteor. Soc.*, **130**, 1171–1194, doi:10.1256/qj.03.133.

Chen, M., W. Shi, P. Xie, V. B. S. Silva, V. E. Kousky, R. W. Higgins, and J. E. Janowiak, 2008: Assessing objective techniques for gauge-based analyses of global daily precipitation. *J. Geophys. Res.*, **113**, D04110, doi:10.1029/2007JD009132.

Cook, B. I., and R. Seager, 2013: The response of the North American Monsoon to increased greenhouse gas forcing. *J. Geophys. Res. Atmos.*, **118**, 1690–1699, doi:10.1002/jgrd.50111.

Corbosiero, K. L., M. J. Dickinson, and L. F. Bosart, 2009: The contribution of eastern North Pacific tropical cyclones to the rainfall climatology of the southwest United States. *Mon. Wea. Rev.*, **137**, 2415–2435, doi:10.1175/2009MWR2768.1.

Dee, D. P., and Coauthors, 2011: The ERA-interim reanalysis: Configuration and performance of the data assimilation system. *Quart. J. Roy. Meteor. Soc.*, **137**, 553–597, doi:10.1002/qj.828.

Delworth, T. L., and Coauthors, 2012: Simulated climate and climate change in the GFDL CM2.5 high-resolution coupled climate model. *J. Climate*, **25**, 2755–2781, doi:10.1175/JCLI-D-11-00316.1.

Douglas, M. W., 1995: The summertime low-level jet over the Gulf of California. *Mon. Wea. Rev.*, **123**, 2334–2347, doi:10.1175/1520-0493(1995)123<2334:TSLLJO>2.0.CO;2.

——, and J. C. Leal, 2003: Summertime surges over the Gulf of California: Aspects of their climatology, mean structure, and evolution from radiosonde, NCEP reanalysis, and rainfall data. *Wea. Forecasting*, **18**, 55–74, doi:10.1175/1520-0434(2003)018<0055:SSOTGO>2.0.CO;2.

——, R. A. Maddox, K. Howard, and S. Reyes, 1993: The Mexican monsoon. *J. Climate*, **6**, 1665–1667, doi:10.1175/1520-0442(1993)006<1665:TMM>2.0.CO;2.

Duchon, C. E., 1979: Lanczos filtering in one and two dimensions. *J. Appl. Meteor.*, **18**, 1016–1022, doi:10.1175/1520-0450(1979)018<1016:LFIOAT>2.0.CO;2.

Erfani, E., and D. Mitchell, 2014: A partial mechanistic understanding of the North American monsoon. *J. Geophys. Res. Atmos.*, **119**, 13 096–13 115, doi:10.1002/2014JD022038.

Favors, J. E., and J. T. Abatzoglou, 2013: Regional surges of monsoonal moisture into the southwestern United States. *Mon. Wea. Rev.*, **141**, 182–191, doi:10.1175/MWR-D-12-00037.1.

Finch, Z. O., and R. H. Johnson, 2010: Observational analysis of an upper-level inverted trough during the 2004 North American monsoon experiment. *Mon. Wea. Rev.*, **138**, 3540–3555, doi:10.1175/2010MWR3369.1.

Fuller, R. D., and D. J. Stensrud, 2000: The relationship between tropical easterly waves and surges over the Gulf of California during the North American monsoon. *Mon. Wea. Rev.*, **128**, 2983–2989, doi:10.1175/1520-0493(2000)128<2983:TRBTEW>2.0.CO;2.

Gilman, D. L., F. J. Fuglister, and J. M. Mitchell Jr., 1963: On the power spectrum of red noise. *J. Atmos. Sci.*, **20**, 182–184, doi:10.1175/1520-0469(1963)020<0182:OTPSON>2.0.CO;2.

Gochis, D., C. Watts, J. Garatuza-Payan, and W. Shuttleworth, 2004: Analysis of 2002 and 2003 warm season precipitation from the North American Monsoon Experiment event rain gauge network. *Mon. Wea. Rev.*, **132**, 2938–2953, doi:10.1175/MWR2838.1.

Hales, J. E., 1972: Surges of maritime tropical air northward over the Gulf of California. *Mon. Wea. Rev.*, **100**, 298–306, doi:10.1175/1520-0493(1972)100<0298:SOMTAN>2.3.CO;2.

Hasson, S., V. Lucarini, and S. Pascale, 2013: Hydrological cycle over South and Southeast Asian river basins as simulated by PCMDI/CMIP3 experiments. *Earth Syst. Dyn.*, **4**, 199–217, doi:10.5194/esd-4-199-2013.

Higgins, R. W., and W. Shi, 2001: Intercomparison of the principal modes of interannual and intraseasonal variability of the North American monsoon system. *J. Climate*, **14**, 403–417, doi:10.1175/1520-0442(2001)014<0403:IOTPMO>2.0.CO;2.

——, and ——, 2005: Relationships between Gulf of California moisture surges and tropical cyclones in the eastern Pacific basin. *J. Climate*, **18**, 4601–4620, doi:10.1175/JCLI3551.1.

——, Y. Yao, and X. L. Wang, 1997: Influence of the North American monsoon system on the U.S. summer precipitation regime. *J. Climate*, **10**, 2600–2622, doi:10.1175/1520-0442(1997)010<2600:IOTNAM>2.0.CO;2.

——, W. Shi, and C. Hain, 2004: Relationships between Gulf of California moisture surges and precipitation in the southwestern United States. *J. Climate*, **17**, 2983–2997, doi:10.1175/1520-0442(2004)017<2983:RBGOCM>2.0.CO;2.

Higgins, W., and D. Gochis, 2007: Synthesis of results from the North American Monsoon Experiment (NAME) process study. *J. Climate*, **20**, 1601–1607, doi:10.1175/JCLI4081.1.

Jiang, X., and N. Lau, 2009: Intraseasonal teleconnection between North American and western North Pacific monsoons with 20-day time scale. *J. Climate*, **21**, 2664–2679, doi:10.1175/2007JCLI2024.1.

——, and D. E. Waliser, 2009: Two dominant subseasonal variability modes of the eastern Pacific ITCZ. *Geophys. Res. Lett.*, **36**, L04704, doi:10.1029/2008GL036820.

Johnson, R. H., P. E. Ciesielski, B. D. McNoldy, P. J. Rogers, and R. K. Taft, 2007: Multiscale variability of the flow during the North American Monsoon Experiment. *J. Climate*, **20**, 1628–1648, doi:10.1175/JCLI4087.1.

Kawamura, R., T. Murakami, and B. Wang, 1996: Tropical and midlatitude 45-day perturbations during the northern summer. *J. Meteor. Soc. Japan*, **74**, 867–890.

Kikuchi, K., and B. Wang, 2009: Global perspective of the Quasi-Biweekly Oscillation. *J. Climate*, **22**, 1340–1359, doi:10.1175/2008JCLI2368.1.

Kiladis, G. N., and E. A. Hall-McKim, 2004: Intraseasonal modulation of precipitation over the North American monsoon region. *15th Symp. on Global Change and Climate Variations*, Seattle, WA, Amer. Meteor. Soc., 11.4. [Available online at http://ams.confex.com/ams/pdfpapers/72428.pdf.]

——, M. C. Wheeler, P. T. Haertel, and K. H. Straub, 2009: Convectively coupled equatorial waves. *Rev. Geophys.*, **47**, RG2003, doi:10.1029/2008RG000266.

Lang, T. J., D. A. Ahijevych, S. W. Nesbitt, R. E. Carbone, S. A. Rutledge, and R. Cifelli, 2007: Radar-observed characteristics of precipitating systems during NAME 2004. *J. Climate*, **20**, 1713–1733, doi:10.1175/JCLI4082.1.

Lee, J.-Y., and B. Wang, 2014: Future change of global monsoon in the CMIP5. *Climate Dyn.*, **42**, 101–119, doi:10.1007/s00382-012-1564-0.

Liepert, B. G., and M. Previdi, 2012: Inter-model variability and biases of the global water cycle in CMIP3 coupled climate models. *Environ. Res. Lett.*, **7**, 014006, doi:10.1088/1748-9326/7/1/014006.

——, and F. Lo, 2013: CMIP5 update of 'Inter-model variability and biases of the global water cycle in CMIP3 coupled climate models.' *Environ. Res. Lett.*, **8**, 029401, doi:10.1088/1748-9326/8/2/029401.

Lorenz, D. J., and D. L. Hartmann, 2006: The effect of the MJO on the North American monsoon. *J. Climate*, **19**, 333–343, doi:10.1175/JCLI3684.1.

Maloney, E. D., and D. L. Hartmann, 2000: Modulation of eastern North Pacific hurricanes by the Madden–Julian oscillation. *J. Climate*, **13**, 1451–1460, doi:10.1175/1520-0442(2000)013<1451:MOENPH>2.0.CO;2.

Mo, K. C., 2000: Intraseasonal modulation of summer precipitation over North America. *Mon. Wea. Rev.*, **128**, 1490–1505, doi:10.1175/1520-0493(2000)128<1490:IMOSPO>2.0.CO;2.

——, and J. Nogues-Paegle, 2005: Pan-america. *Intraseasonal Variability in the Atmosphere-Ocean Climate System*, K. M. Lau and D. E. Waliser, Eds., Springer-Verlag, 95–124.

Mullen, S. L., J. T. Schmitz, and N. O. Rennó, 1998: Intraseasonal variability of the summer monsoon over southeast Arizona. *Mon. Wea. Rev.*, **126**, 3016–3035, doi:10.1175/1520-0493(1998)126<3016:IVOTSM>2.0.CO;2.

Newman, A. J., and R. H. Johnson, 2012a: Mechanisms for precipitation enhancement in a North American monsoon upper-tropospheric trough. *J. Atmos. Sci.*, **69**, 1775–1792, doi:10.1175/JAS-D-11-0223.1.

——, and ——, 2012b: Simulation of a North American monsoon gulf surge event and comparison to observations. *Mon. Wea. Rev.*, **140**, 2534–2554, doi:10.1175/MWR-D-11-00223.1.

——, and ——, 2013: Dynamics of a simulated North American monsoon gulf surge event. *Mon. Wea. Rev.*, **141**, 3238–3253, doi:10.1175/MWR-D-12-00294.1.

Nolin, A. W., and E. A. Hall-McKim, 2006: Frequency modes of monsoon precipitation in Arizona and New Mexico. *Mon. Wea. Rev.*, **134**, 3774–3781, doi:10.1175/MWR3244.1.

Pascale, S., V. Lucarini, X. Feng, A. Porporato, and S. Hasson, 2016: Projected changes of rainfall seasonality and dry spells in a high greenhouse gas emissions scenario. *Climate Dyn.*, **46**, 1331–1350, doi:10.1007/s00382-015-2648-4.

Pytlak, E., M. Goering, and A. Bennett, 2005: Upper tropospheric troughs and their interaction with the North American monsoon. *19th Conf. on Hydrology*, San Diego, CA, Amer. Meteor. Soc., P2.3. [Available online at https://ams.confex.com/ams/pdfpapers/85393.pdf.]

Rienecker, M. M., and Coauthors, 2011: MERRA: NASA's Modern-Era Retrospective analysis for Research and Applications. *J. Climate*, **24**, 3624–3648, doi:10.1175/JCLI-D-11-00015.1.

Rogers, P. J., and R. H. Johnson, 2007: Analysis of the 13–14 July gulf surge event during the 2004 North American Monsoon Experiment. *Mon. Wea. Rev.*, **135**, 3098–3117, doi:10.1175/MWR3450.1.

Schiffer, N. J., and S. W. Nesbit, 2012: Flow, moisture, and thermodynamic variability associated with Gulf of California surges within the North American monsoon. *J. Climate*, **25**, 4220–4241, doi:10.1175/JCLI-D-11-00266.1.

Seastrand, S., Y. Serra, C. Castro, and E. Ritchie, 2015: The dominant synoptic-scale modes of North American monsoon precipitation. *Int. J. Climatol.*, **35**, 2019–2032, doi:10.1002/joc.4104.

Serra, Y. L., G. N. Kiladis, and K. I. Hodges, 2010: Tracking and mean structure of easterly waves over the Intra-Americas sea. *J. Climate*, **23**, 4823–4840, doi:10.1175/2010JCLI3223.1.

Stensrud, D. J., R. L. Gall, and M. K. Nordquist, 1997: Surges over the Gulf of California during the Mexican monsoon. *Mon. Wea. Rev.*, **125**, 417–437, doi:10.1175/1520-0493(1997)125<0417:SOTGOC>2.0.CO;2.

Svoma, B. M., 2010: The influence of monsoonal gulf surges on precipitation and diurnal precipitation patterns in central Arizona. *Wea. Forecasting*, **25**, 281–289, doi:10.1175/2009WAF2222299.1.

Taylor, K. E., R. J. Stouffer, and G. A. Meehl, 2012: An overview of CMIP5 and the experiment design. *Bull. Amer. Meteor. Soc.*, **93**, 485–498, doi:10.1175/BAMS-D-11-00094.1.

Vecchi, G. A., and Coauthors, 2014: On the seasonal forecasting of regional tropical cyclone activity. *J. Climate*, **27**, 7994–8016, doi:10.1175/JCLI-D-14-00158.1.

Wood, K. M., and E. A. Ritchie, 2013: An updated climatology of tropical cyclone impacts on the southwestern United States. *Mon. Wea. Rev.*, **141**, 4322–4336, doi:10.1175/MWR-D-13-00078.1.

Wu, M.-L. C., S. D. Schubert, M. J. Suarez, and N. E. Huang, 2009: An analysis of moisture fluxes into the Gulf of California. *J. Climate*, **22**, 2216–2239, doi:10.1175/2008JCLI2525.1.

Zehnder, J. A., 1991: The interaction of planetary-scale tropical easterly waves with topography: A mechanism for the initiation of tropical cyclones. *J. Atmos. Sci.*, **48**, 1217–1230, doi:10.1175/1520-0469(1991)048<1217:TIOPST>2.0.CO;2.

——, 2004: Dynamic mechanisms of the Gulf surge. *J. Geophys. Res.*, **109**, D10107, doi:10.1029/2004JD004616.

——, D. M. Powell, and D. L. Ropp, 1999: The interaction of easterly waves, orography, and the intertropical convergence zone in the genesis of eastern Pacific tropical cyclones. *Mon. Wea. Rev.*, **127**, 1566–1585, doi:10.1175/1520-0493(1999)127<1566:TIOEWO>2.0.CO;2.